Villanova University
The Graduate School
Department of Civil and Environmental Engineering

Evaporation from A Pervious Concrete Stormwater SCM: Estimating the Quantity and its Role in the Yearly Water Budget

A Thesis in
Civil Engineering
by
Evgeny M. Nemirovsky, PE

Submitted in partial fulfillment
of the requirements
for the degree of
Master of Science
May 2011

Evaporation from A Pervious Concrete Stormwater SCM: Estimating the Quantity and its Role in the Yearly Water Budget

by

Evgeny M. Nemirovsky, PE

May 2011

Andrea Welker, Ph.D., P.E. Associate Professor of Civil and Environmental Engineering	Date
Robert Traver, Ph.D., P.E. Professor of Civil and Environmental Engineering	Date
Ronald A. Chadderton, Ph.D., P.E. Chairman, Department of Civil and Environmental Engineering	Date
Gary A. Gabriele, Ph.D. Dean, College of Engineering	Date

Acknowledgements

I feel very fortunate to be a part of the flagship water resources program at Villanova University. I had an opportunity to work with the wonderful, most knowledgeable and passionate people, whose influences would always stay with me.

I am very grateful to my advisors, Dr. Andrea Welker and Dr. Robert Traver, for their guidance, insight, help, and trust. Their encouragement and support made this work possible.

I would like to acknowledge Mr. Ryan Lee for the vital advice, and Dr. Francis Hampton, Dr. Metin Duran, Mr. George Pappas, and Mr. Chris Townend for their help, direction and resources.

I want to thank Dr. John Kevern of University of Missouri-Kansas City and Dr. Vernon Schaeffer of Iowa State University for their collaboration and selfless sharing of the experimental data.

I want to thank Dr. Bridget Wadzuk, Dr. Qianhong Wu, Dr. Alfonso Ortega, Dr. Amy Fleischer, Dr. Komlos, Dr. Pritpal Singh, Dr. Aleksandra Radlinska, Dr. Joseph Yost, Dr. Ronald Chadderton, Ms. Sonali Joshi, Ms. Linda DeAngelis, and Mr. John Stofey for their advice, help, resources, and valuable critique.

I want to extend my thanks to Dilsad Yilmazel, Sevda Alanya, Shane Moran, Noelle Helmstetter, Erika DeFonce, Katie Thomas, and Caitlin McEntee for their assistance with the experiment.

I want to acknowledge my colleagues: Kevin Flynn, James Pittman, Kaitlin Vacca, Kathryn Greising, Mike Hickman, Dominik Schneider, and Sarah Fjell for their help and camaraderie.

Special thanks go to my father, Dr. Michael Nemirovsky, for the collaboration, example and enthusiasm, and to the rest of my family: Mom, Sasha, and Jenya for being very close despite nearly 5,000 miles between us.

Finally, and most importantly, I am forever grateful to my wife, Yesim Ay, for her unreserved support, patience and love.

Abstract

Use of pervious pavements as stormwater control measures (SCMs) or best management practices (BMPs) is a well-established practice. These pavements, when used in conjunction with infiltration beds, are effective at reducing runoff volume, improving water quality, recharging the ground water table, and mitigating high temperature inflows. Flow reduction mechanisms are based on capture and temporary storage of runoff in the stone bed beneath pervious pavements and subsequent infiltration through subsurface soils. Evaporation is another potential mechanism through which temporarily stored runoff is released; however, it is neglected as a design practice due to limited knowledge and apparent insignificance.

The research described here was conducted to identify parameters affecting evaporation rates from a pervious concrete SCM, measure evaporation in a laboratory setting, and predict typical evaporation rates from pervious concrete SCMs. This work describes the design of a pervious concrete bench-top scale model and its evaporation behavior in response to simulated environmental conditions. The results from this experiment indicate that daily evaporation rates vary substantially with change in depth to the ponded water within the SCM. Evaporation behavior in fully saturated conditions resembled that of an open water body. The ponded water had an influence zone of 10 inches (254 mm) beyond which its effect on evaporation behavior was insignificant. The results of this work indicate that evaporation can play a significant role in the hydrologic performance of shallow SCMs with poor or inhibited ground infiltration characteristics.

Table of Contents

List of Figures

List of Tables

1. Introduction

1.1 Porous pavements as stormwater BMP

Use of porous pavements as a stormwater BMP is a well-established practice. Pervious concrete and asphalt were first used as stomwater management devices in the 1970's (Ferguson 2005) since then their popularity had been growing. PA Stormwater BMP Manual (PADEP 2006) defines permeable pavements as "permeable surface course underlain by a uniformly-graded stone bed which provides temporary storage for peak rate control and promotes infiltration. The surface course may consist of porous asphalt, porous concrete, or various porous structural pavers laid on uncompacted soil". Benefits of pavements include, but are not limited to reduction in runoff rates, ground water recharge, improvement in runoff water quality, heat island effect mitigation, and runoff temperature mitigation.

1.2 Mechanisms of runoff release

Flow reduction mechanisms are based on temporary storage of runoff in the stone bed and subsequent infiltration through subsurface soils. The rate of infiltration depends on soil parameters, temperature, degree of saturation, water quality, and other parameters (Viessman and Lewis 2003). The mechanism is not fully understood, but the phenomenon is relatively well studied. Estimates for site-specific infiltration are available from literature.

Evaporation is another mechanism through which temporarily stored runoff is released from the stone bed. However, due to perceived insignificance and limited knowledge of evaporation rates through pervious pavement surfaces, this mechanism is neglected. Pervious pavement designs resulting from this approach are conservative because they omit evaporation. Evaporation from pervious pavements, on the other hand, is not well established. Some research was performed in the past on this subject, which is reviewed in Section 2.

1.3 Research objectives

The objective of this work was to study evaporation behavior of pervious concrete systems using a bench-top simulation. The goals were to identify parameters affecting evaporation rates and to establish functional relationships that would predict evaporation behavior. Evaporation rates representative for typical summer conditions in the Philadelphia area were sought. The research also included assessment of the evaporation performance of pervious concrete SCMs, and its role in a yearly BMP water budget. The final objective of this work was to revisit the BMP design guidelines in light of the findings, and provide recommendations if applicable.

1.4 Pervious pavement BMP site at Villanova University

In 2007 a conventional asphalt parking lot at Villanova University was retrofitted to serve as pervious pavement research BMP (Barbis and Welker 2010). Two pervious sections (concrete and asphalt) were constructed side by side following design guidelines prescribed by the PA Stormwater BMP manual (PADEP 2006). Stormwater performance is being monitored and comparative analysis is being reported. The laboratory setup to achieve the research objective was modeled after the pervious concrete portion of this site, however, it is believed that the experiment is sufficiently generic for non-site-specific applications. **Figure 1.1** provides an overview of Villanova University pervious pavement BMP research site.

Figure 1.1 VU pervious pavement BMP site

2. Literature review

2.1 Evapotranspiration vs. evaporation

Assessment of water vapor losses from a stormwater BMP depends on the type of management practice. In vegetated BMPs (e.g. bioretention cells, green roofs, bio-swales) evaporation from open water body is concurrent with the plant's transpiration. Consequently, these mechanisms are combined into one category - evapotranspiration. In case of non-vegetated BMPs such as porous pavements with storage beds, water vapor losses are limited to evaporation only. Although the settings do not closely match evaporation from an open body of water, the mechanisms of vapor transfer are similar. For the purpose of this study, loss of water through the pores of pervious pavement will be referred to as evaporation.

2.2 Evaporation

Evaporation is defined as "net rate of vapor transfer" (Viessman and Lewis 2003). Evaporation from an open body of water is a function of the solar radiation, difference in vapor pressure, temperature, wind, atmospheric pressure, and physical and chemical properties of water.

For open water bodies, evaporation potential is equal to 100%. For soil and other porous media, evaporation also depends on the moisture content, as well as the other factors mentioned above. Evaporation potential is reported to vary from 100% in saturated conditions to nearly zero at low moisture contents.

2.3 Annual evaporation from shallow water bodies

Annual evaporation from shallow lakes and reservoirs play an important role in the water budget. In the US, mean annual evaporation varies from about 15 inches to 110 inches (381 mm to 2794 mm) depending on geographic region. For example, mean annual evaporation from shallow lakes and reservoirs in Philadelphia, PA is about 35 inches (889 mm) (NOAA 1982). Compared to a 30-year average annual precipitation of 42.85

inches for the same area (NOAA 1971-2000), evaporation constitutes 81.7% of a yearly water budget.

2.4 Potential evaporation calculation techniques

Methods for the estimation of the potential evaporation include using a water budget, energy budget, mass transfer, and use of evaporation pans. (Viessman and Lewis 2003). Energy budget and mass transfer methods require the most instrumentation and maintenance effort for representative measurements. Water budget and evaporation pan techniques are more common due to relative ease of data collection.

Of the mass transfer techniques, an empirical method developed by Meyer is commonly used:

Equation 2.1 Meyer daily evaporation

$$E=C(e_o-e_a)(1+W/10)$$, where:

E = daily evaporation in inches of depth
e_o = saturation vapor pressure at water surface temperature, in inches of Hg
e_a = vapor pressure of the air, in inches of Hg
W = wind velocity 25 ft above water surface, in mph
C = pan empirical coefficient

Another method is developed by Dunne:

Equation 2.2 Dunne daily evaporation

$$E=(0.013+0.00016u_2)e_a[(100-RH)/100]$$, where:

E = evaporation rate in cm/day
u_2 = wind velocity measured at 2 m above surface in km/day
e_a = vapor pressure of the air, in millibars
RH = relative humidity in percent

The evaporation pan method is most widely used in finding the reservoir evaporation. In this technique, pan evaporation is adjusted by a reduction factor (pan coefficient varying from 0.70 to 0.75) to compute reservoir evaporation. National Weather Bureau Class A Evaporation Pan is currently the most popular pan. Class A daily pan evaporation, assuming air and water temperature are equal, is calculated using the following equations:

Equation 2.3 Class A daily pan evaporation

$$E_a = (e_o - e_a)^{0.88}(0.42+0.0029u_p), \text{ and}$$

Equation 2.4 Vapor pressure difference

$$(e_o - e_a) = 33.86[(0.00738T_a+0.8072)^8-(0.00738T_d+0.8072)^8], \text{ where:}$$

$(e_o - e_a)$ = vapor pressure difference in millibars
u_p = wind movement 150 mm above the rim of the pan in km/day
T_a = air temperature in degrees C
T_d = dew point temperature in degrees C (valid for $T_d >= -27$ deg C)

There are additional methods (e.g. Penman and Kohler) that are built upon the pan evaporation technique to derive daily evaporation.

2.5 Evaporation from pervious pavements

A number of studies on evaporation from pervious pavements were published in recent years. The majority of them investigate evaporation to assess its affect on the temperature of the porous medium. The primary objective of a few publications was to investigate evaporation rates. No physics or statistics-based model predicting evaporation from pervious pavements was found.

The most comprehensive study that was found to date is currently being conducted at University of Munster, Germany (Starke, Göbel and Coldewey 2010). The objective of this research was to "vary and optimize the characteristics of water-permeable pavements (structure and constitution of the road base, underlay, structure and constitution of the

paving stones used, width and filling of the seams, etc.) taking into consideration the applicable regulations, in such as way as to achieve evaporation rates that are as high and as constant as possible". This is a full-scale study designed and constructed to satisfy research objectives. Evaporation rates were measured in-situ using a newly developed tunnel evaporation gauge (German name is Tunnelverdunstungsmessgerät or TUV), which operates by comparing relative humidity just above the surface as air enters and leaves a half-cylinder "tunnel" positioned over the pavement. The system had an underdrain which prevented any ponding of water to occur. Therefore, the study did not account for a water surface contribution to the total evaporation. This study is ongoing; the results published to date include surfaces comprised of cobble stone, concrete paving stone and pervious concrete paving stone with pervious seams, but not cast-in-place pervious concrete slabs. Other related publications, presented in **Table 2.1**, discuss evaporation from pervious surfaces directly or indirectly.

Table 2.1 Publications on evaporation

Reference	Summary
Takashi Asaeda, Vu Thanh Ca, "Characteristics of permeable pavement during hot summer weather and impact on the thermal environment", Building and Environment 35 (2000), pp 363-375	This article discusses temperature reduction in porous surfaces as compared to non-porous surfaces.
C. Bordier, D. Zimmer, "Drainage equations and non-Darcian modelling in coarse porous media or geosynthetic materials", Journal of Hydrology 228 (2000), pp 174-187	This paper describes an analytical approach to flow equations in coarse porous media.
M.R. Hall, D. Allinson, "Evaporative drying in stabilized compressed earth materials using unsaturated flow theory", Building and Environment	This work investigates evaporative drying in compressed earth materials such as earth bricks, and rammed earth walls. Sorbtion and desorbtion mechanisms investigated. This work

45 (2010), pp 509–518	provides good insight into mechanisms of evaporative drying.
Surakha Wanphen, Katsunori Nagano, "Experimental study of the performance of porous materials to moderate the roof surface temperature by its evaporative cooling effect", Building and Environment 44 (2009), pp 338– 351	This paper investigates evaporative cooling effect of porous roofing materials. Among tested materials were: silica sand, volcanic ash, siliceous shale, and pebbles. Equipment setup was devised utilizing mass transfer principles. Relative humidity and temperature of the chamber were controlled, while weight and surface temperature was monitored.
Takashi Asaeda and Vu Thanh Ca, "Heat storage of pavement and its effect on the lower atmosphere", Atmospheric Environment Vol. 30 No 3 (1996), pp. 413-427	This work focuses on the heat storage capacity of the pavement and how it affects urban warming. Temperature behavior of asphalt, concrete, and bare soils was evaluated.
Paul D. Tennis, Michael L. Leming, and David J. Akers, "Pervious concrete pavements", PCA (2004)	This PCA publication describes design, construction and maintenance techniques for pervious concrete pavements. Notably, in the section on hydrologic design *evaporation* is not mentioned in any form.
C. T. Andersen, I. D. L. Foster and C. J. Pratt, "The role of urban surfaces (permeable pavements) in regulating drainage and evaporation: development of a laboratory simulation experiment", Hydrological Processes 13 (1999), pp 597-609	This work reported results from a laboratory simulation designed to mimic hydrologic and hydraulic performance of a pervious pavement system. A model was developed using paver blocks on top of stone, with water infiltration and evaporation occurring through the joints between the blocks. The system was equipped with a rain simulator. Variable parameters were bed grain size and bed depth. Evaporation and infiltration were measured using mass transfer principles. Potential evaporation was estimated

	using pans, and related to the actual evaporation.
"North Carolina State University evaluates Permeable Pavements", D. R. Smith, K. A. Collins and W.F. Hunt III, Interlocking Concrete Pavement Magazine (2006), pp 18-23.	In this publication, four types of permeable pavements (including pervious concrete) are studied for runoff water quality and quantity. In conclusion, the authors mention that "runoff volumes are likely reduced from the base storage, soil infiltration and evaporation".

3. Methods

In this section the approach and details of the experiment design, methods, and instrumentation utilized to achieve research objective are described.

3.1 Prototype

A pervious pavement research SCM site at Villanova University was used as a prototype for the laboratory experiment. The experimental setup to study evaporation performance was modeled after the pervious concrete section of this research site. Several aspects of the SCM performance were assessed for accurate representation in the scaled model.

3.1.1 Materials and hydrologic performance

The tributary drainage area of the pervious concrete portion of the Villanova SCM is approximately 3,920 ft^2 (364.4 m^2). The pervious area itself measures 1,500 ft^2 (139.4 m^2), therefore the stormwater loading ratio is 3,920:1,500 or 2.61:1. The profile of the pervious concrete pavement system at VU consisted of a 6 inch (152 mm) thick pervious concrete layer and a 36 inch (914 mm) thick (on average) aggregate bed underlain by a non-woven geotextile fabric atop of the existing soil. Refer to **Figure 3.1** for a typical pervious concrete system profile.

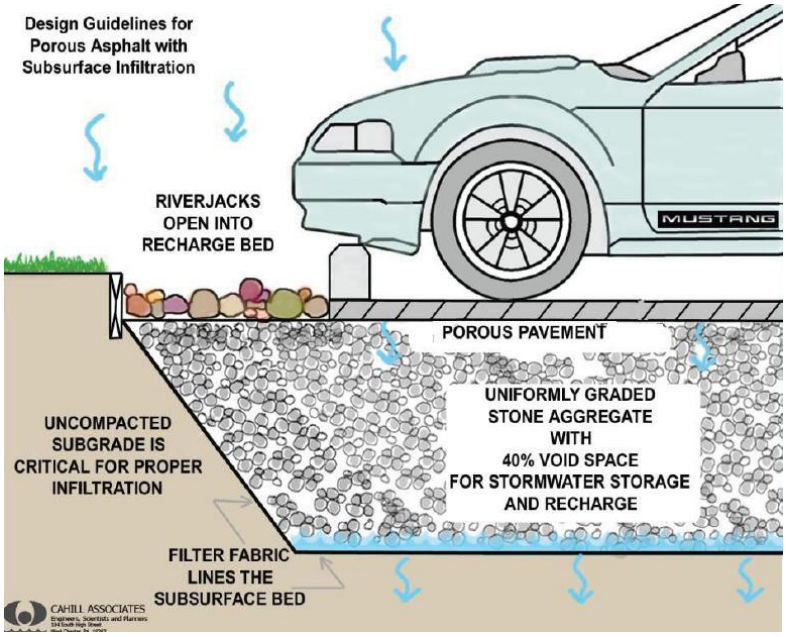

Figure 3.1 Pervious concrete system profile (Cahill / PADEP, 2006)

Ponded water levels within this SCM fluctuate in response to rainstorm events. Rainfall event over 2 inches (51 mm) would fill the system to the capacity and would produce overflow conditions. Average infiltration observed over the monitoring period was about 0.5 inches/hour (13 mm/hour) (Jeffers 2009).

Details on material dimensions and properties are outlined in **Table 3.1**.

3.1.2 Temperature response

In addition to material considerations, temperature data was collected at this research site to be incorporated into behavior of bench-top model. Surface temperature and the temperature at a depth of 40 inches (1016 mm) were recorded using I-Button sensors and INW Pressure/Temperature probe.

3.1.3 Solar radiation, ambient temperature, wind, and relative humidity

Solar radiation, ambient temperature, wind velocity and relative humidity at the site were continuously monitored. The sensors and data were maintained by Villanova University Weather Center (Mendel Weather Station 2010).

3.2 Profile composition

Design of the experimental apparatus focused on replicating the vertical composition and dimensions while the horizontal dimension was scaled to 4 inches (102 mm) diameter. The constructed profile consisted of a pervious concrete layer and an aggregate layer. Several such setups were built during this investigation. The first version of the apparatus with scaled vertical dimensions was built as a proof of concept. The final version of the setup was constructed by replicating a non-scaled vertical profile for in-depth investigation (**Table 3.1**).

Table 3.1 Comparative profile composition

	VU SCM site*	**Experimental apparatus: proof of concept**	**Experimental apparatus: final version**
Top layer			
Material	Pervious concrete	Pervious concrete	Pervious concrete
Thickness	6 inches (152 mm)	3 inches (76 mm)	6 inches (152 mm)
Porosity	0.15 - 0.2 **	0.2	0.2
Hydraulic conductivity	7-20 m/hr **	24.8 m/hr (6.95×10^{-3} m/s)	24.8 m/hr (6.95×10^{-3} m/s)
Aggregate layer			
Material	AASHTO #57 stone	AASHTO #57 stone	AASHTO #57 stone
Thickness	36 inches (914 mm) (average)	11 inches (279 mm)	36 inches (914 mm)
Porosity	About 0.40	About 0.40	About 0.40

* (Jeffers 2009)

** (Tennis, Leming and Akers 2004)

3.3 Experimental apparatus: proof of concept

To achieve the research objective, it was necessary to design an experiment that would simulate evaporation behavior in pervious concrete systems. To this end it was necessary to build a scaled model of a prototype site, recreate the driving force behind the

evaporation process (solar radiation), simulate conditions of the system in response to rainstorm events (variable depth to ponded water), control or report environmental conditions (temperature, wind and relative humidity) and assess the loss of water vapor from the system.

The first version of the apparatus with scaled vertical dimensions was built to demonstrate that the concept behind the experiment design and the instrumentation selected for this task would yield sensible data. A core resembling a profile of the Villanova pervious concrete SCM was built inside a water-tight PVC cylinder with an internal diameter of 4 inches (102 mm). The concrete layer was 3 inches (76 mm) thick and aggregate layer was 11 inches (279 mm) thick. Refer to **Table 3.1** for material details.

The hydrologic response of the system to stormwater events was simulated by controlling the initial depth to ponded water within the system (measured from the top surface). This was achieved by saturating the apparatus with tap water and then draining the water to the required initial depth. The hydrologic response associated with just-after-the-rainstorm conditions was achieved in that ponded water reached a prescribed elevation and pore spaces above ponded water were moist.

The evaporation behavior was induced by subjecting the concrete surface to radiation from a halogen work light which had a significant amount of by-product heat. For the proof-of-concept stage of the experiment, the light was used in a steady-state mode (constant power output), which does not have the characteristics of a daily solar pattern but is indicative enough for demonstration purposes.

The evaporation performance was isolated from infiltration by inhibiting the horizontal and downward vertical routes of water transport by water-tight construction of the apparatus. Consequently, the top layer of the pervious concrete provided for the only route of water vapor transfer in an upward direction.

Evaporation was assessed by employing mass transfer principles; therefore a scale with sufficient resolution (0.1 gram) was utilized to perform the measurement. The weight of the apparatus was continuously monitored using a digital balance with streaming data output. The change in weight was attributed exclusively to water vapor transfer through the pores of the pervious concrete layer (i.e. evaporation).

The experiment was conducted in a laboratory environment and ambient and surface temperature and relative humidity (RH) were monitored during the experiment using data-logging sensors (**Figure 3.2**).

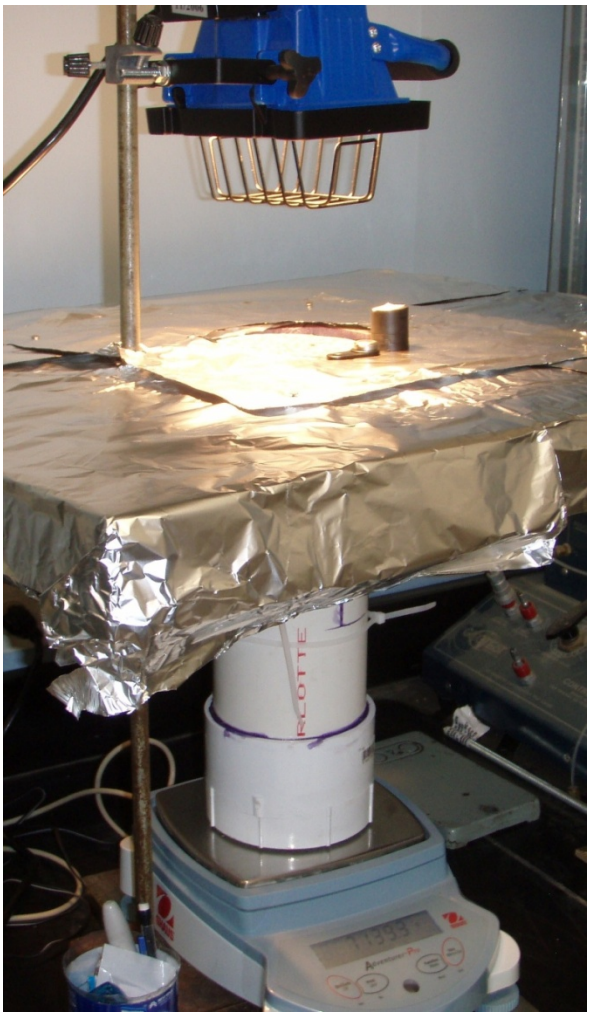

Figure 3.2 Experimental apparatus: proof-of-concept

The photograph shown in **Figure 3.2** shows the apparatus positioned on digital scale. The work light is suspended directly above the surface comprised of the pervious concrete layer. The temperature and relative humidity sensors are located adjacent to the concrete surface on top of a platform suspended independently of evaporation cylinder. The platform featuring the circular opening was made of insulating foam to allow for flush no-touch penetration of the evaporation cylinder. Refer to Section 3.10 for details on the instrumentation.

Several preliminary runs were performed during the proof-of-concept stage of the experiment. The initial depth to ponded water for each run was varied from zero to 10 inches (254 mm). The results presented in **Figure 3.3** were from a 48-hour run with an initial depth to ponded water of 5 inches (127 mm).

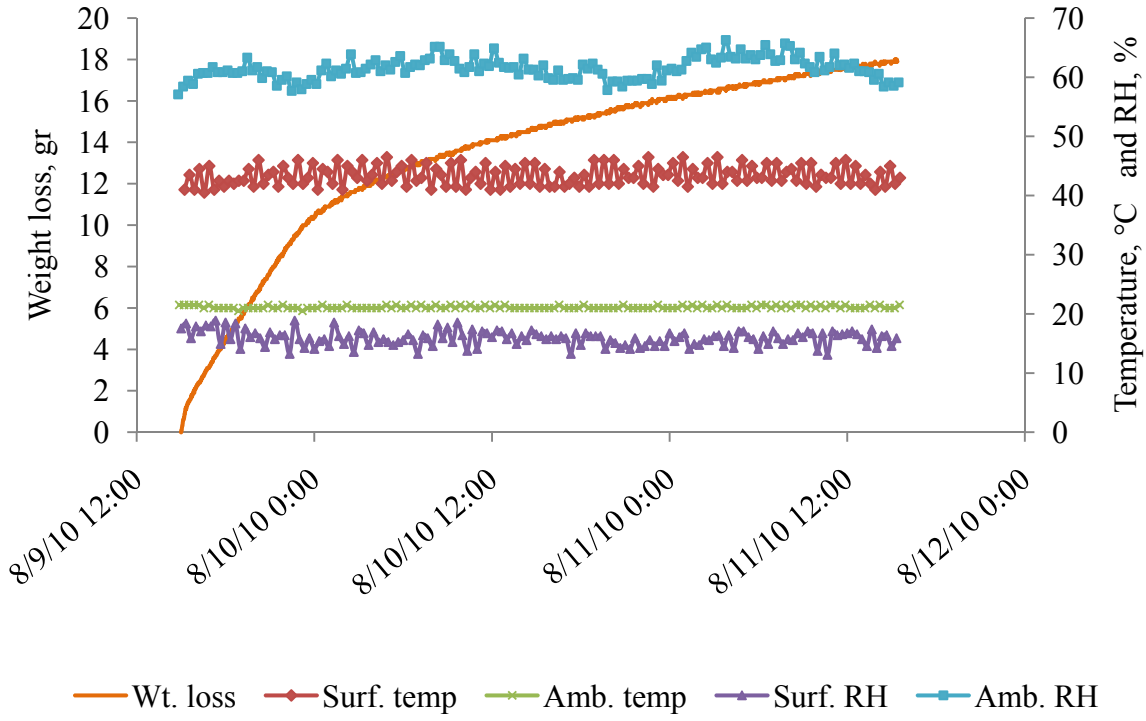

Figure 3.3 System weight loss, initial depth to water: 5 inches (127 mm)

The data shown in **Figure 3.4** indicate that the 48-hour cumulative weight loss for the system with initial depth to ponded water equal to 5 inches (127 mm), with a constant

temperature regime is 18 grams. The results were translated in terms of the evaporation from a free water surface using surface area of the core and water density. **Figure 3.4** shows the results in terms of the equivalent free surface evaporation in millimeters.

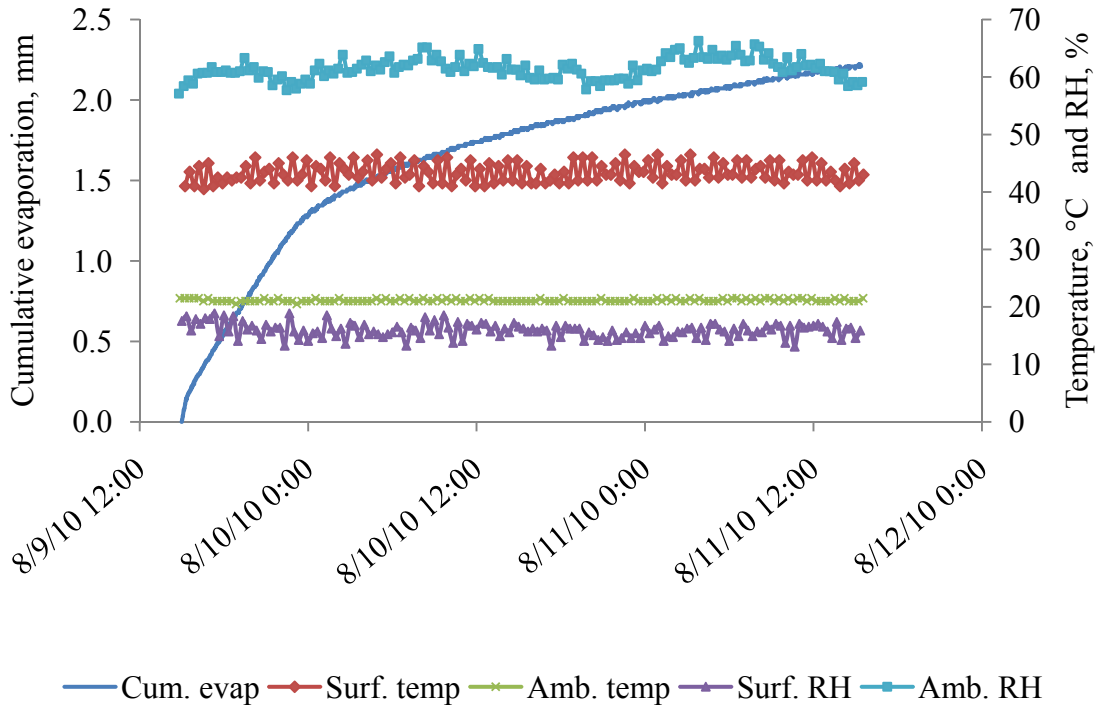

Figure 3.4 System evaporation, initial depth to water: 5 inches (127 mm)

As evident from the results, the cumulative 48-hour evaporation for the given conditions was 2.2 mm. The evaporation rate slowed down significantly as the time progressed.

The magnitude of the obtained weight-based evaporation results was substantially greater than the resolution of the measuring device, and the character of the evaporation rates was easily discernible and in line with the expectations. Therefore, it was concluded that the conceptual design of this experiment and selected instrumentation could, in principle, satisfy the research objective.

3.4 Heat transfer considerations

It was reasoned that in a homogenous (in the horizontal axis) pervious pavement system heat transfer occurs in the vertical direction only, because all horizontal layers in the system receive an equal amount of heat from solar radiation. Therefore, to create a scaled model with thermal behavior matching field conditions, the horizontal heat flux had to be prevented or minimized.

Additionally, heat transfer in the vertical direction results in a distinct thermal profile which is unique for different points in yearly and daily cycles. The thermal profile representative for conditions in the field had to be established to obtain a representative scale model.

To assess the thermal behavior of the setup in general and the horizontal heat transfer in particular, infra-red spectrum images were taken with a FLIR thermal camera (**Figure 3.5**).

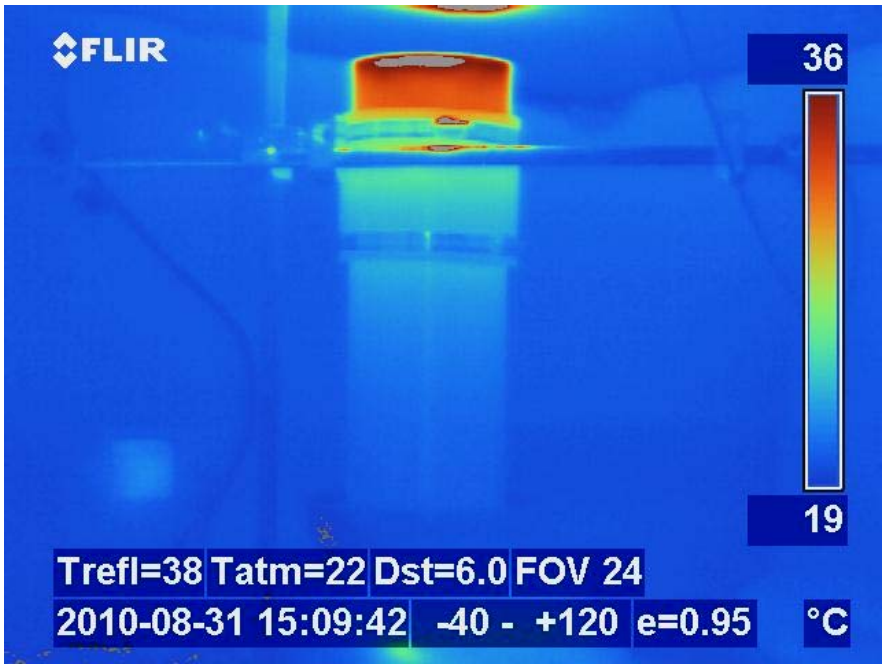

Figure 3.5 Infra-red image: proof-of-concept apparatus

Inspection of the isotherms revealed that the edges of the column were several degrees cooler than the core. This was evidence of horizontal heat flux, which had to be prevented to appropriately model field conditions. Consequently, the column was insulated with R-13 fiberglass insulation to inhibit the horizontal component of heat transfer.

The effectiveness of this method was verified using measurements from four Omega E-Type thermocouples embedded at different depths into the column while being positioned at the same vertical distance from the top surface (see Section 3.10 for details on instrumentation). The instrumentation layout is presented in **Figure 3.6**.

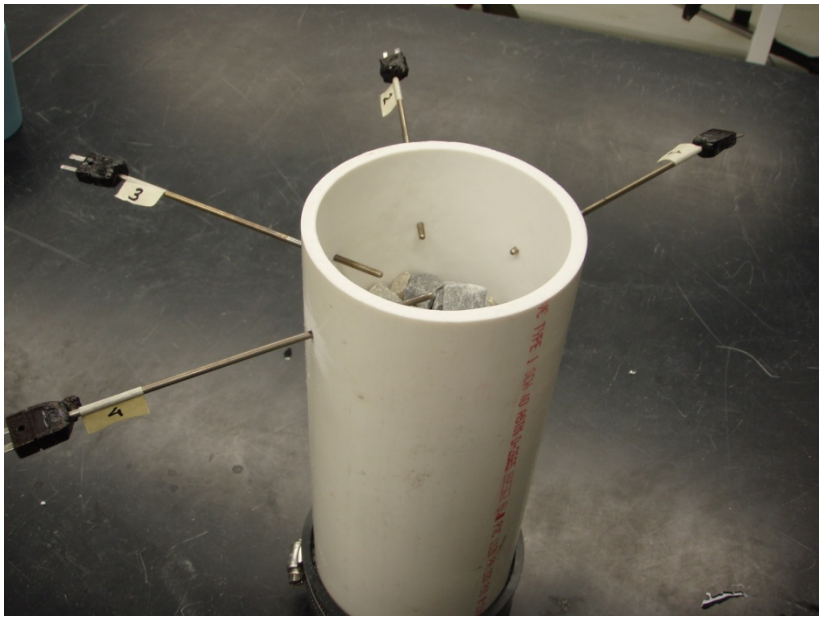

Figure 3.6 Horizontal heat flux: testing

The picture in **Figure 3.6**.shows protruding thermocouples imbedded in the column prior to being filled with the aggregate. **Figure 3.7** shows the insulated apparatus.

Figure 3.7 Horizontal heat flux: insulated apparatus

The apparatus was heated with a steady-state output halogen work light. Temperature changes in the horizontal direction were monitored using discrete measurements with a Tegan thermocouple reader (see Section 3.10.4 for details). It was observed that the temperature was hottest at the column center and coldest near the wall. However, temperature variation in the horizontal plane was found to be less than 1° C, therefore horizontal heat flux was considered insignificant for the purposes of this experiment.

In contrast to preventing heat flux in the horizontal direction, the conditions for vertical heat transfer had to be created to replicate conditions in the field. The bottom of the column was made of a thermally conductive material (brass) to promote cooling of the lower layers of the "aggregate bed" to the ambient room temperature, which was kept constant. The bottom of the apparatus was kept un-insulated to facilitate heat exchange in the vertical direction between the heat source (work light heating the top surface) and heat sink (bottom exposed to the ambient temperature). The heat transfer details, temperature behavior of a prototype pervious pavement site and calibration of the thermal profile in the experimental setup will be discussed in Sections 3.5 and 4.

3.5 Thermal profile considerations

The nitial version of the experimental apparatus did not address the issues pertaining to the cyclic nature of a temperature response and the thermal profile development in pervious pavement systems. It was observed that with a steady-state heat source, the temperature response of the experimental setup reaches steady-state equilibrium within about 6 to 18 hours from the session start, depending on the initial depth to the ponded water surface.

The temperature response of a pervious concrete system in the field, on the other hand, is substantially more complex. It is never at a steady-state thermally because an incident solar radiation varies as the sun "moves" along its daily trajectory.

The need for a solar simulator became evident when daily and seasonal fluctuations in the temperature of the pervious pavement systems were realized. A soil temperature model developed at Oklahoma State University (Nofziger and Wu 2005) and a recent study on temperature behavior of a pervious concrete system at Iowa State University (Kevern et al. 2009) provided detailed insight into the development of a thermal profile typical for pervious concrete BMPs. The soil temperature model illustrated average daily changes in the temperature of the surficial layers that occur as a result of seasonal earth cycles. At a particular depth (about 12 meters from the surface in temperate climate zone), soil temperature is approximately constant throughout the year (at about 14° C). This phenomenon occurs as the soil medium reaches thermal equilibrium between a "constant" heat source inside earth's core and a heat sink of seasonally variable temperature that surrounds the planet. Average daily temperatures in the surface layers vary in response to seasonal cycles, and the amplitude of this fluctuation increases as the point of interest approaches the surface. **Figure 3.8** shows average daily temperature behavior throughout the year. Surface temperature and temperatures at 0.5 m and 1 m depth are plotted. **Figure 3.9** shows the average daily thermal profiles typical for January 1 and August 1 of any given year.

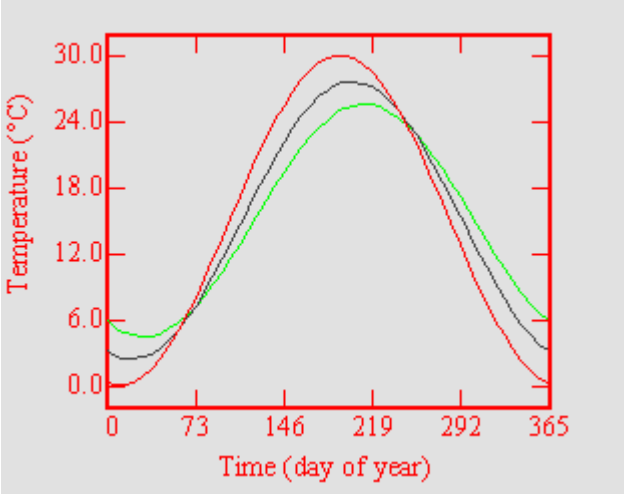

Figure 3.8 Average daily temperature during the year (Nofziger and Wu 2005)

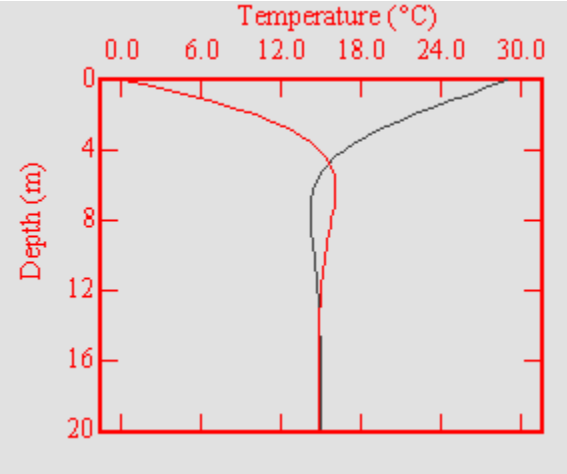

Figure 3.9 Average daily thermal profiles, Jan-1 and Aug-1 (Nofziger and Wu 2005)

In addition to seasonal changes, temperatures at the surface layers fluctuate daily. The study of a pervious concrete system in Iowa demonstrated that the amplitude of daily temperature fluctuations near the surface could be as much as 20° C, with the effects of daily surface temperature swings propagating as much as 55 cm below the surface (Kevern et al. 2009). **Figure 3.10** illustrates daily temperature fluctuations at various depths throughout the pervious concrete system in the summer.

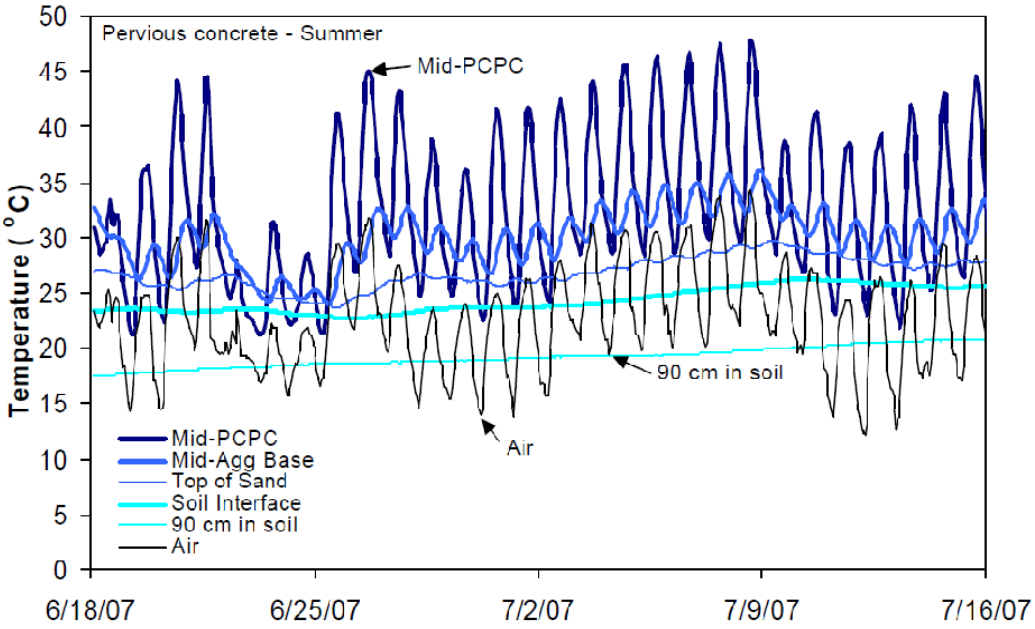

Figure 3.10 Daily temperature fluctuations (Kevern et al. 2009)

These considerations revealed the complexity of temperature behavior of pervious concrete systems, which could not be simulated in laboratory setting by a steady-state heat source. It was necessary to build a solar simulator that would mimic the daily solar cycle observed at the prototype site by providing a variable heat output throughout the day. It was hypothesized that by subjecting the surface to a variable radiation representative of a daily solar cycle, a temperature behavior typical for the surface layers of a pervious concrete system would be achieved in the experimental setup. Sections 3.10.16 and 4.5 will discuss the details of the solar simulator design, operation and calibration.

3.6 Hydrologic response considerations

Pervious concrete systems exhibit a complex response to a precipitation event. Water or water vapor crosses the system boundary as a result of precipitation, infiltration and evaporation. Temperature fluctuation and other factors can make the rate of those processes variable.

For the purpose of this study, the infiltration mechanism was not included in the experiment design. Therefore, any moisture or water vapor transfer was possible only

through simulated precipitation (refill of the system with water) or through the induced evaporation process.

In field conditions, the end of a rainstorm event is characterized by a particular ponded water surface elevation - an instantaneous equilibrium point resulting from inflow of runoff and direct precipitation through the pervious surface and infiltration through the bottom or sides of the structure which lowers the surface of ponded water. Because any significant rainstorm event would result in direct precipitation and runoff from adjacent impervious areas entering in top-down fashion onto the pervious pavement system, it was reasoned that the inter-pore spaces of pervious concrete or aggregate that are above the ponded water level will be completely moist at the end of the storm.

These two considerations identified the objectives of the initiation of each experimental run: a prescribed water elevation and moist above-water inter-pore spaces. The manner in which each experimental run would be initialized was designed to satisfy those objectives. Because it was desirable to have inter-pore spaces completely moist at the start of each data collection session, the setup was momentarily filled with room-temperature tap water to saturation. Then, to obtain the required ponded water elevation, the water was drained to the prescribed level.

3.7 Ambient temperature and relative humidity considerations

Ambient temperature and relative humidity significantly affect evaporation behavior (see Section 2.4). Experiments conducted during the proof-of-concept stage of this research showed that the relative humidity in the laboratory environment can vary substantially even if the HVAC system is centrally controlled. The change in humidity occurred as fresh air of variable humidity and temperature was drawn in from the outside, resulting in inconsistent humidity inside the laboratory. To isolate these unaccounted for factors, in was desired to control ambient conditions at constant levels, typical for the average conditions in the field.

3.8 Wind considerations

Wind is an important factor that affects evaporation behavior (see Section 2.4). To get representative evaporation behavior in the laboratory setting, wind conditions typical for the field conditions were replicated. Historical wind data at the site was available: average near-surface wind velocity in the summer was about 300 feet/minute (1.5 meters/second). Wind conditions were replicated in the experimental setup.

3.9 Experimental apparatus: final design

The final design of the experimental apparatus addressed considerations identified during the proof-of-concept stage. Horizontal heat flux inhibition and approximation of the hydrologic response typical for the field conditions were incorporated. Substantial effort was dedicated to replicating the cyclic nature of the thermal response of the pervious concrete system which results from daily fluctuations in solar radiation. Scaling of the model in the vertical dimension was eliminated: depths of the pervious concrete layer and the aggregate layer were replicated based on the measurements from the prototype site. Inconsistencies in ambient temperature and relative humidity were resolved, and wind considerations were addressed.

The new apparatus was built featuring the same horizontal dimension (internal diameter of 4 inches (102 mm)) as the initial setup, and the vertical dimension measuring 42 inches (1067 mm).

Four pervious concrete specimens measuring 4 inches (102 mm) in internal diameter, and 6 inches (152 mm) in depth were cast inside pre-cut schedule 40 PVC pipe segments. The concrete mix was designed by Dr. F. Hampton of Villanova University. Concrete was cast per ASTM Standard Practice for Sampling Freshly Mixed Concrete (ASTM 2010). Details on the mix design are presented in **APPENDIX A**. **Figure 3.11** is a photograph of one of the freshly cast specimens located in the curing room.

Figure 3.11 Pervious concrete specimen

Upon curing, laboratory testing was performed to determine the porosity and hydraulic conductivity of the specimens. The porosity was found using a water displacement method. The hydraulic conductivity was found using a modified constant head infiltration test. **Table 3.2** provides the material properties determined from the tests.

Table 3.2 Porosity and hydraulic conductivity

Sample ID	Porosity	Hydraulic conductivity, cm/second
4A	0.20	0.68
4B	0.15	0.58
4C	0.16	0.57
4D	0.20	0.69

The pervious concrete specimen designated 4D with a porosity of 0.20 was used in the apparatus assembly. The pervious concrete specimen was attached to the aggregate section of the apparatus using a Fernco flexible coupling with the inside diameter of 4.5

inches (114 mm) – matching that of the PVC pipe outside diameter. The resulting connection was durable and water-tight. **Figure 3.12** is a stock photo of the coupling.

Figure 3.12 Fernco flexible coupling

The aggregate section of the apparatus was filled with AASHTO #57 stone, similarly to the material at the VU BMP prototype site. The material was supplied by Galantino Supply Company, Inc of Springfield, PA. The gradation analysis of the aggregate is presented in **APPENDIX B**.

The apparatus was insulated with Pink Fiberglass™ insulation by Owens Corning Insulating Systems, LLC. The insulation had an R-value of 13, roll width of 15 inchs (381 mm), and material thickness of 3.5 inches (89 mm). The insulation was cut and assembled into rings using duct tape to fit around the cylinder. Two 15 inch (381 mm) wide rings and one 12 inch (305 mm) wide rings were stacked vertically to insulate the entire side surface area of the apparatus.

The bottom of the apparatus was equipped with an Oatey 4 inch (102 mm) diameter brass cleanout plug with recessed head to promote cooling of the lower layers of the apparatus. The brass plug was fitted onto a 4 inches (102 mm) diameter PVC cleanout adapter manufactured by Nibco attached to the main column of the apparatus. All PVC-to-PVC joints were sealed with PVC Cement by Oatey. All metal-to-PVC joints were sealed with Sikaflex®-1a polyurethane elastomeric sealant/adhesive manufactured by Sika Corporation.

The apparatus was equipped with a drain, also functioning as a piezometric well, installed 2 inches (51 mm) above the bottom of the column. A watts 1/4 inch x 3/8 inch (6.4 mm x 9.5 mm) brass hose barb x MIP adapter was threaded into the wall of the apparatus and sealed with Sikaflex®-1a sealant. Watts 1/4 inch (6.4 mm) PVC tubing was attached to the barbed connection and run vertically to the top of the apparatus.

To eliminate drainage conditions resulting in vertical plug flow throughout the entire column and the consequent disruption of the established thermal profile, an additional drainage assembly was installed 10 inches (254 mm) below the top surface to accommodate the draining performed at the initiation of each experiment run (**Figure 3.13**).

The atmospheric opening of both tubing assemblies was clamped shut at the beginning of each data collecting session to prevent additional evaporation from the water surface in the tube.

To monitor the thermal response of the system, five thermocouples were installed throughout the column connected to a thermocouple data logger. Four E-type Omega sheathed thermocouples were embedded in the center of the core at the depths of 3, 15, 28 and 40 inches (76, 381, 711 and 1016 mm) while one K-type bare-wire thermocouple was located at the pervious concrete surface. Thermocouple penetrations through the PVC shell of the column were sealed with Sikaflex®-1a polyurethane sealant to assure water-tight construction. All thermocouples were connected to a Pico TC-08 data logger by Pico Technology. Refer to Sections 3.10.3 and 3.10.5 for details on the thermocouples and the data logger.

The ambient temperature, ambient relative humidity and surface relative humidity were monitored with I-Button Thermochron and Hygrochron devices manufactured by Dallas Semiconductors. Refer to Section 3.10.2 for the product specifications.

The change in the weight of the system (and, thereby, the system's evaporation response) was measured with digital industrial bench scale (model GP-61K manufactured by A&D). The scale was connected to a laptop PC where streaming weight data output was recorded. Sections 3.10.8 and 3.10.9 present details on the scale and computer operation.

The final version of the apparatus featured a solar simulator in place of a steady-state heat source utilized in the proof-of-concept phase. A solar simulator was built to replicate the daily temperature fluctuations which occur at the top layers of a pervious pavement system in response to solar radiation varying in the course of a day. Components of the solar simulator included a halogen lamp (a directional heat source) controlled by a power switching device (a solid state relay) which in turn was controlled by a computer via software developed for this purpose. The solar simulator operates by matching the lamp output at any given time interval to a daily solar radiation curve observed at the VU pervious pavement BMP site. This is achieved by continuously switching the lamp into the ON and OFF positions for the appropriate duration and delay interval. Section 3.10.16 elaborates on the details of the solar simulator design and on the calibration of the thermal response of the apparatus to that of the prototype site. Refer to **Figure 3.13** for the details on components of the apparatus.

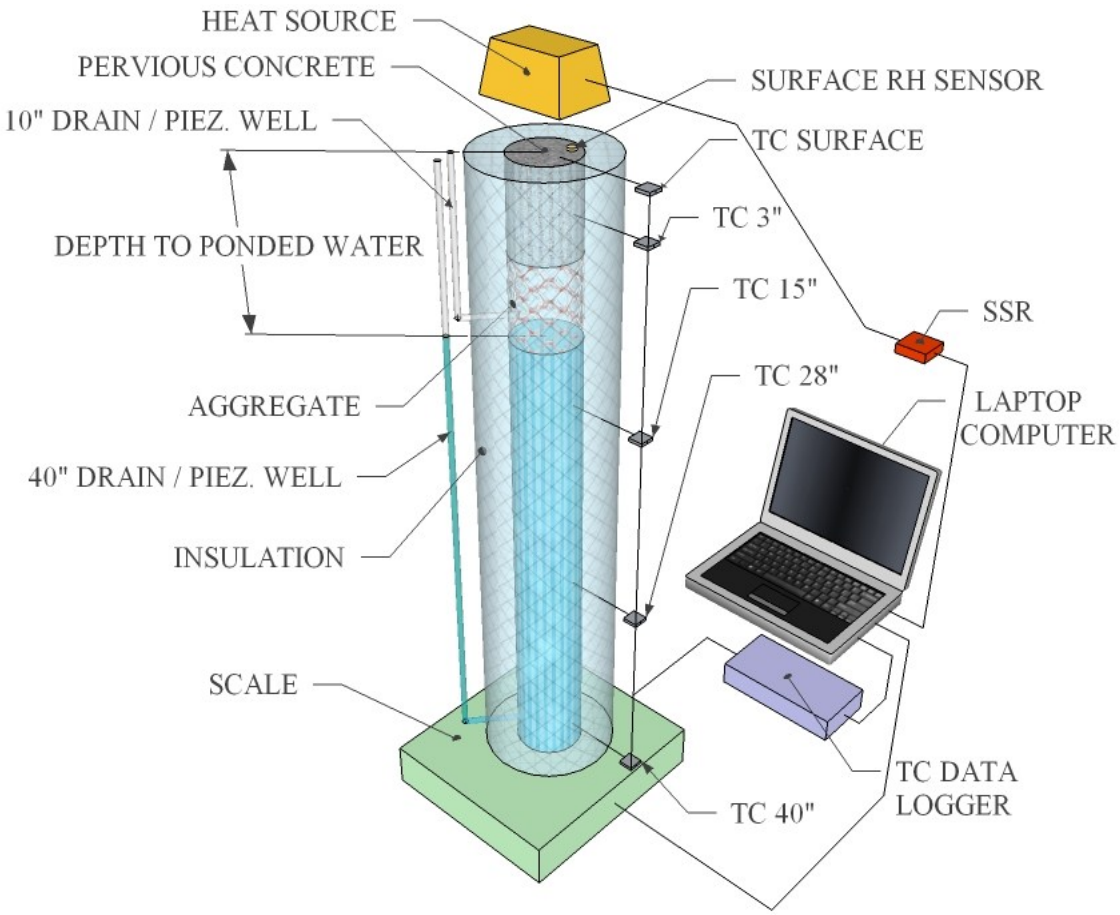

Figure 3.13 Experimental apparatus: final design

To address inconsistencies in the ambient temperature and relative humidity during data collection sessions, the apparatus was moved into an environmental room located in SETRL (Structural Engineering Technological Research Laboratory). Ambient temperature was set to 21° C and relative humidity to 50%.

To incorporate wind into the experimental system, a wind tunnel was built. The tunnel performed two functions: it provided a channel for development of laminar flow over the pervious concrete surface and shielded the apparatus from uncontrolled air currents resulting from normal operation of the environmental room. Near-surface wind induced by a fan was about 300 feet per second (1.5 meters/second). Refer to Section 3.10.13 for the details on the wind tunnel design. **Figure 3.14** is a photograph of the apparatus, with

the wind tunnel incorporated, during (access door closed) and just after (door opened) data collection session.

Figure 3.14 (a, b) Complete apparatus

3.10 Instrumentation

Among the instrumentation used to control and monitor the environmental factors in the laboratory setting were temperature sensors, relative humidity sensors, thermocouples, a thermocouple reader, a thermocouple a data logger, a digital balance, a laptop PC, an anemometer, an environmental room, a wind tunnel, an infrared camera, and a solar simulator.

3.10.1 Temperature sensor

An I-Button Thermochron DS1921G by Dallas Semiconductors (**Figure 3.15**) was used for the purpose of temperature monitoring. The device is capable of data gathering and logging at a set interval. The data logging capacity of the device is 2048 data entries. The following characteristics are taken from the technical specifications:

- Temperature reading resolution is 0.5°C
- Accuracy ±1°C from -30°C to +70°C

Communication with the device was performed utilizing a USB-based interface with a laptop PC. The software interface "I-Button Viewer" developed by Dallas Semiconductors was used for logged data retrieval and missions setup.

Figure 3.15 I-Button Thermochron

3.10.2 Relative humidity / temperature sensor

I-Button Hygrochron DS1923#F5 device by Dallas Semiconductors (**Figure 3.16**) was used for the purpose of relative humidity (RH) monitoring. In addition to RH, the device is capable of temperature monitoring as well. The device logs data at a set interval. The total data logging capacity of the device is 8192 or 4096 data entries depending on the chosen data resolution. The following characteristics are taken from the product technical specifications:

- RH reading resolution is 0.04% or 0.6%
- Operating range: from -20°C to +85°C
- RH accuracy: ±5 %
- Temperature reading resolution is 0.0625°C or 0.5°C
- Temperature accuracy ±0.5°C from -10°C to +65°C

Figure 3.16 I-Button Hygrochron

Communication with the device was performed utilizing a USB-based interface with a laptop PC. The software interface "OneWireViewer" developed by Dallas Semiconductors was used for logged data retrieval and missions setup.

3.10.3 Thermocouples

Temperature measurements at the surface of the experimental apparatus and throughout its depth were obtained using thermocouples. For the surface measurements, K-type wire thermocouples, AWG 30 (0.255 mm diameter), with exposed tip, glass braid insulation, and standard miniature connector were used (**Figure 3.17**).

Figure 3.17 K-type thermocouple

Omega E-type thermocouples, 0.062 inches (1.57 mm) in diameter, 6 inches (152 mm) long, grounded, with stainless steel sheath and standard miniature connector were used for temperature measurements below surface (**Figure 3.18**).

Figure 3.18 Omega E-type thermocouple

3.10.4 Thermocouple calibrator-thermometer

Tegam Inc. digital temperature calibrator-thermometer model 841 (**Figure 3.19**) was used to verify horizontal heat flux inhibition. The readings were taken manually at discrete intervals from thermocouples installed as described in Section 3.4. Following specification details were provided by the manufacturer:

- Supported thermocouple types: K, J, T, E, N, B, R, S, G, C, D.
- K range: -200°C to 1372°C, -328°F to 2502°F
- E range: -230°C to 1000°C, -382°F to 1832°F

- Accuracy (18°C to 28°C ambient, 2 years)*:
  K, J, T, E, N; ± 0.5°F (rdg ≥ -50°F) ±1.0°F (rdg < -50°F)
  * Exclusive of sensor errors, and lead resistance induced errors.
- Temperature resolution: 0.1 °/1° F/C
- Repeatability (1 week at constant ambient temperature):
  K, J, T, E, N; ± 0.2°F typ.

Figure 3.19 Thermocouple calibrator-thermometer

3.10.5 Thermocouple data logger

Pico Technology model USB TC-08 thermocouple data logger (**Figure 3.20**) was used to obtain fine increment data of the thermal response. The data logger was equipped with eight (8) channels for simultaneous data acquisition from multiple thermocouples. The data logger was connected to a laptop PC (Section 3.10.9) via a USB cable which also served as a power source. The interface was through a software program PicoLog release 5.21.2 by Pico Technology Ltd. Using the software interface, each channel was configured and the data sampling interval was set. The session data was stored at the specified location on the laptop PC. At the end of each session the data was exported to a data processing application. The following is an excerpt from the product specifications:

- Supported thermocouple types: B, E, J, K, N, R, S, T
- Conversion time - per active channel: 100 ms
- Conversion time – CJC: 100 ms

- Uncalibrated accuracy: The sum of ±0.2% and ±0.5°C
- Environmental conditions: 0 to 50°C, 25% to 75% humidity
- Actual measurable / theoretical range for Type E thermocouple: -270°C to 910°C / -270°C to 910°C
- Actual measurable range for Type K thermocouple: -270°C to 1370°C / -270°C to 1370°C

Figure 3.20 Thermocouple data logger

3.10.6 Pressure/temperature data logger

Instrumentation Northwest PT2X submersible pressure/temperature smart sensors (**Figure 3.21**) were used to record the subsurface temperature at the Villanova pervious concrete system. The device had the following characteristics:

- Typical accuracy: ± 0.06% FSO
- Data logging: pressure, temperature, time
- Memory capacity: 130,000 - 520,000 records
- Power: 2 internal AA batteries

Figure 3.21 Pressure/temperature data logger

The devices were programmed to collect the data at 10-minute intervals. Communication with the device was through a RS485 cable connected to a R-232 port on the laptop PC.

The interface was performed through Aqua4Plus control software by Instrumentation Northwest. Upon upload, the recorded data was imported into Excel spreadsheets for processing.

3.10.7 Digital balance 1

Ohaus Adventurer-Pro AV8101 (**Figure 3.22**) was one of the digital balances utilized in the experiment. It was used in the proof of concept stage of experimentation to monitor changes in the sample weight. The following specifications characterize the device performance:

- Readability: 0.1 g
- Repeatability: 0.1 g
- Linearity: +/- 0.2 g
- Capacity: 8,100 g
- Stabilization time: 2 s

Communication with the balance was via a RS-232 cable connecting the respective ports of the device and the laptop PC. The software interface for data collection and storage was HyperTerminal by Microsoft Corporation. The data was taken at discrete one-minute intervals and sent to HyperTerminal software for temporary storage in random-access memory (RAM). Every five minutes, RAM data from HyperTerminal was uploaded and appended to a data file on laptop PC's hard drive.

Figure 3.22 Digital balance 1

3.10.8 Digital balance 2

An A&D GP-61K Industrial Bench Scale (**Figure 3.23**) was used to monitor changes in the sample weight during the deployment stage of the experiment. The following specifications characterize the device performance:

- Capacity: 61,000 g
- Resolution: 0.1 g
- Linearity: +/- 0.5 g
- Repeatability / Std. dev: 0.2 g
- Stabilization time: 1.5 s

Communication with the balance was via a RS-232 cable connecting the respective ports of the device and the laptop PC. The software interface for data collection and storage was HyperTerminal by Microsoft Corporation. The data was taken at discrete intervals (approximately 5.3 seconds apart) and sent to the HyperTerminal software for temporary storage in random-access memory (RAM). Every five minutes RAM data from HyperTerminal was uploaded and appended to a delimited text data file on laptop PC's hard drive. After completion of each session, text delimited data was imported to a spreadsheet (Microsoft 2007) for data processing.

Figure 3.23 Digital balance 2

3.10.9 Laptop PC

A Dell Latitude 610 laptop PC with Microsoft Windows XP SP3 operating system was used for communication with the RH / temperature sensors and digital scale (**Figure 3.24**). RS-232 and USB ports were used as the input/output interface.

Figure 3.24 Laptop computer

3.10.10 Anemometer

Wind speed measurements were performed with a stopwatch-bucket mechanical vane anemometer, manufactured by Tycos of Rochester, NY (**Figure 3.25**). The device reports in-stream air flow velocity, in feet, corresponding to a time interval measured using a stopwatch. One revolution of the needle on the dial face equals to 100 feet (30.5 meters). All measurements were performed using a one minute interval, therefore the measurement units were feet per minute.

Figure 3.25 Anemometer

3.10.11 Stopwatch

Extech Stopwatch/Clock #365515 was used for the measurement of the time intervals to obtain the wind speed (**Figure 3.26**). The stopwatch accuracy was +/- 3 seconds per 24 hours.

Figure 3.26 Stopwatch

3.10.12 Environmental room

An environmental room was used to control the temperature and relative humidity during the experiment. The room measured approximately 24 ft x 24 ft x 12 ft (7.3 m x 7.3 m x 3.3 m). Control of the humidity at a set level was performed utilizing a humidifier and dehumidifier working concurrently through a feedback loop. The temperature was controlled similarly through an air conditioning unit and heating unit connected to a central controller. The room featured six 20 inch (0.5 meter) diameter fans working continuously for uniform humidity and temperature distribution. The following specifications describe the operating accuracy of the system:

- Temperature: +/- 0.5° C
- RH: +/- 2%

3.10.13 Wind tunnel

The wind tunnel was designed to mimic average wind behavior observed at the Villanova pervious pavement SCM site. The primary function of the wind tunnel was to aid in the development of controlled laminar air flow over the evaporation surface. Additionally, the wind tunnel shielded the evaporation surface from uncontrolled air currents and eddies resulting from the fans, which were necessary for the operation of the

environmental room. The wind tunnel was custom built from 3/8 inch (9.5 mm) thick plywood. The structure consisted of a support leg – a vertical box, which encased the scale and the column, and a wind tunnel – a horizontal box with a circular opening in the bottom face to accommodate a flush, no-touch penetration of the evaporation surface (**Figure 3.27**). A 16 inch (406 mm) diameter fan was attached to one of the flanges of the wind tunnel to promote air flow through the box. For access, the structure was furnished with a hinged door, allowing access to the instrumentation below the evaporation surface and the evaporation surface itself. The structure had the following dimensions:

- Support leg footprint: 26 inches x 20 inches (660 mm x 508 mm)
- Support leg height: 52 inches (1321 mm)
- Wind tunnel cross section: 20 inches x 20 inches (508 mm x 508 mm)
- Wind tunnel length: 78 inches (1981 mm)
- Door: 26 inches x 73 inches (660 mm x 1852 mm)
- Bottom face circular opening diameter: 9 inches (229 mm)

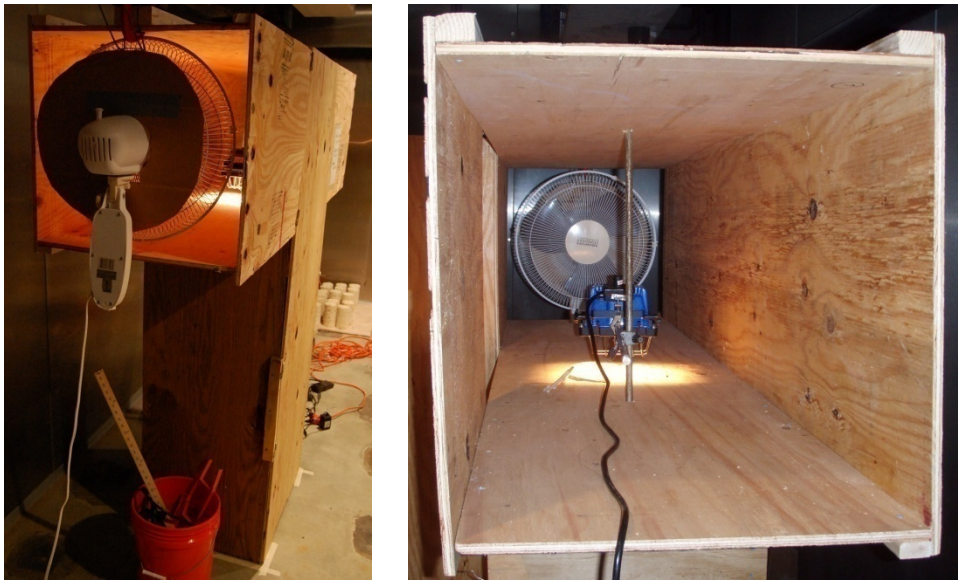

Figure 3.27 (a, b) Wind tunnel

3.10.14 Fan

A Home Essentials 16 inch (406 mm) diameter fan with three adjustable rotor speed settings was used in the wind tunnel (**Figure 3.27**).

3.10.15 Infrared camera

A FLIR ThermaCam P25 thermal camera was used to obtain infra-red spectrum images to assess the performance of the experimental apparatus (**Figure 3.28**). The camera had the following characteristics.

- Temperature ranges: -40° C to +120° C (-40° F to +248° F),
  0° C to +500° C (+32° F to 932° F)
- Accuracy (% of reading): ± 2° C or ± 2%
- Field of view/min focus distance: 24° x 18° / 0.3 m
- Spatial resolution (IFOV): 1.3 mrad
- Thermal sensitivity @ 50/60Hz: 0.08° C at 30° C
- Spectral range: 7.5 to 13 µm

Figure 3.28 Thermal camera

3.10.16 Solar simulator

The solar simulator was built to replicate the daily temperature fluctuations which occur at top layers of pervious pavement systems in response to a daily varying solar radiation. Components of the solar simulator included the halogen lamp which was controlled by a solid state relay (SSR), which in turn was controlled by a computer program running on the laptop PC (see Section 3.10.9).

The simulator operates on the principle of pulse modulation, by adjusting the lamp output at any given time interval to a daily solar radiation curve. Within one time interval the

lamp output is comprised of the discrete pulses of constant power, variable duration (ON cycle) and variable delay (OFF cycle). For any given time of the day, the duration of the ON cycle is proportional to the ratio of present time solar radiation to the maximum daily solar radiation (occurring at solar noon). Consequently, the lamp is on 100% of time at time intervals near solar noon and off 100% of time from sunset to sunrise. For all other time intervals, the duration of the ON cycle varies from 0 to 100%. **Figure 3.29** is a simplified diagram of the solar simulator operation principle, showing one 24-hour cycle.

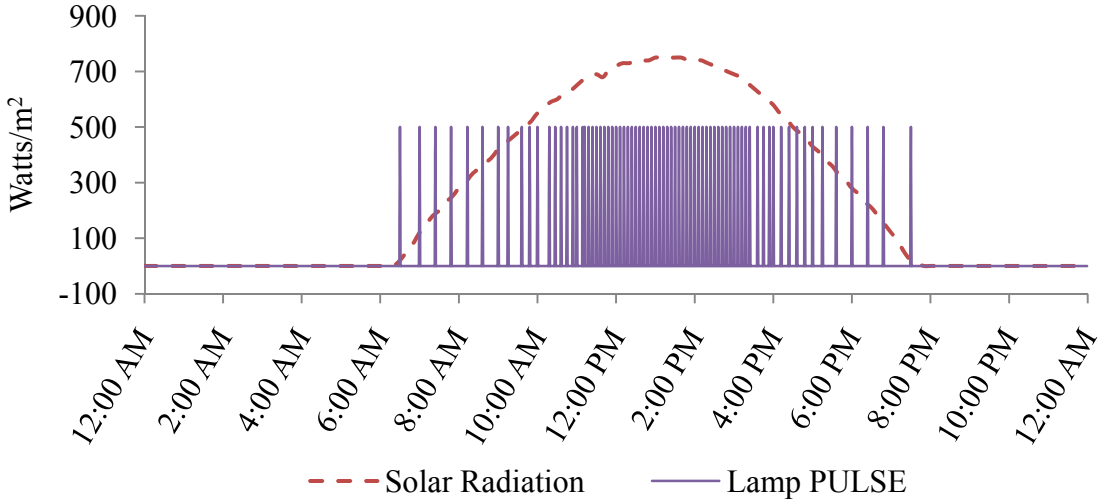

Figure 3.29 Solar simulator: pulse modulation

The lamp used for this setup was a WorkForce portable work light with a halogen bulb (**Figure 3.30**). The lamp had two power settings: 125 W and 250 W. Calibration of the maximum surface temperature was performed by changing the power output and by changing the distance from the lamp to the surface of the apparatus.

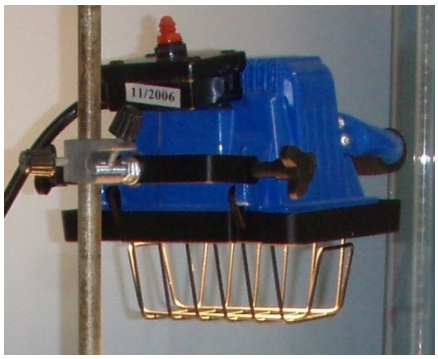

Figure 3.30 Lamp / Heat source

The SSR was used as a power switching device to turn the lamp on and off at the prescribed times and for the specified durations (**Figure 3.31**). The SSR had the following specifications:

- Control voltage: 3-27 VDC
- Load power: 10 AMP, 24-280 VAC
- Operating Temperature: -20 to 80°C
- Storage Temperature: -40 to 80°C
- Isolation: 4000 Vrms, input to output; 2500 Vrms input/output to ground
- Capacitance: 8 pF, input to output (max)
- Line Frequency Range: 47 to 63 Hz
- Turn-On Time: 20 ms, AC; 05 cycle, DC
- Turn-Off Time: 30 ms, AC; 05 cycle, DC

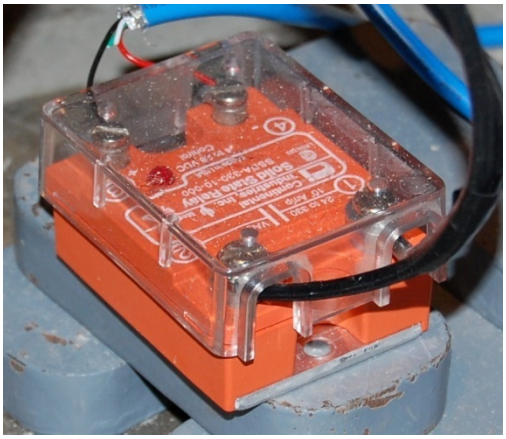

Figure 3.31 Solid state relay

The SSR was connected to and controlled through a LPT (printer) port on the laptop PC. **Figure 3.13** provides the wiring schematics. A control program, SolarSimulator 1.1, was written in Visual Basic specifically for this application (see **Figure 3.32** for the screenshot). The algorithm for this program was based on the solar simulator operation logic described earlier in this section. A block diagram outlining the algorithm is presented in the **APPENDIX C**.

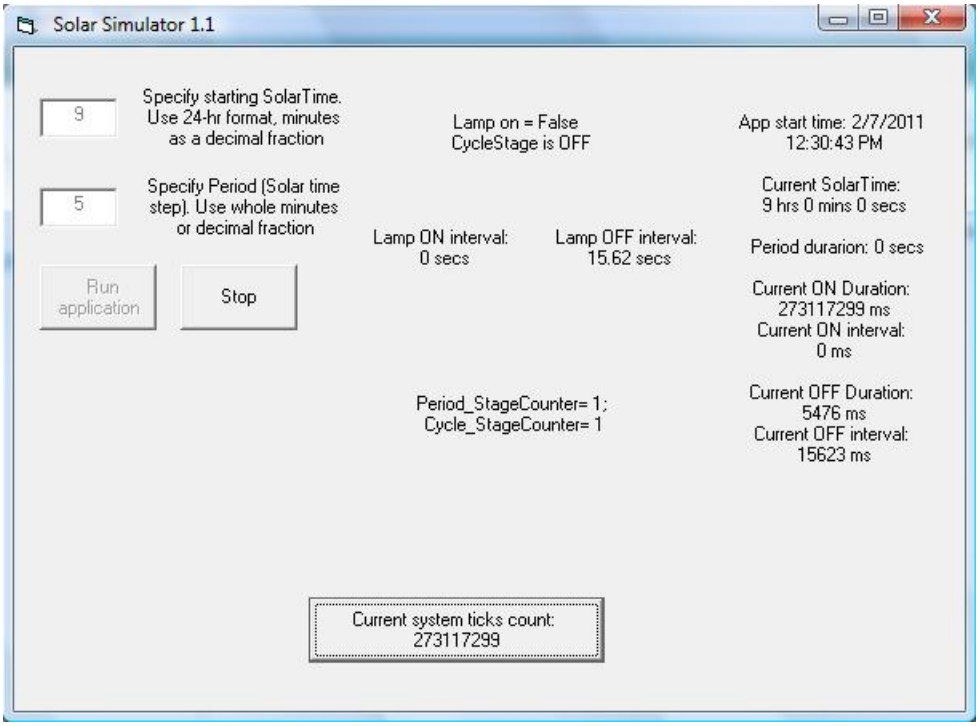

Figure 3.32 Solar Simulator 1.1 screenshot

3.11 Experimentation program

The experimentation program's objective was to study the evaporation response which would occur during three typical clear summer days immediately following a rainstorm event. Several "rain" scenarios were used, resulting in a different pre-set initial depth to ponded water (measured from the pervious concrete surface). Besides the study of the evaporation response, the program was designed to find the limiting depth to ponded water surface beyond which the change in evaporation rates is insignificant.

Data collection was performed in sessions. For each session the recorded data included: ambient, surface and below-surface temperature; ambient and surface relative humidity; and surface wind velocity.

The solar simulator ran continuously for the entire duration of the experiment, assuring that the thermal response was repeatable and replicated the field conditions. Each simulation started at the same time, 30 minutes prior to solar noon (±5 minutes) and lasted for 72 hours (3 days).

3.11.1 Sessions identification

All data collection sessions during the experiment had nearly identical environmental parameters, which were controlled centrally: ambient temperature, ambient relative humidity, near-surface wind velocity, and the amount and timing of radiation delivered by the solar simulator. The sessions were differentiated by varying initial depths to ponded water.

Six simulations were performed, each having a different initial depth to water. Saturated conditions (initial depth of 0 inches (0 mm)) and depths equal to 1, 3, 6, 10 and 15 inches (25, 76, 152, 254, and 381 mm) were simulated.

3.11.2 Session initialization

Each simulation was initialized in a consistent manner to maintain similar initial conditions. Initialization considerations included minimizing changes to the thermal equilibrium and assuring moist above-water pore spaces (refer to Section 3.6 for details). Initialization consisted of simulating the end of the rainstorm conditions by adding tap water to the assembly through the pores of the pervious concrete layer to establish a prescribed depth to the water surface.

To ensure that the initial thermal and hydrologic conditions for each run are equal, the following protocol was established and implemented before each simulation:

a) Verify that the apparatus is in thermal equilibrium (i.e. it had been subjected to heat from the solar simulator for two consecutive days or more)
b) Drain the water to a depth of 10 inches (254 mm) below surface
c) Momentarily refill the apparatus to saturation with tap water at approximately 20° C
d) Drain the water to the required depth
e) Start recording the session data

Drainage of the water from the apparatus (when applicable) was performed first using a drain located at 10 inches (254 mm) below surface, and then, if needed, using the drain

located at 40 inches (1016 mm) below surface. This sequence was developed to minimize disruption to the previously established thermal profile.

3.11.3 Reporting of the results

Evaporation results were reported in millimeters of water lost over the equivalent area of a free water surface. It must be noted that the actual drop in the ponded water elevation was considerably greater. For water levels within the concrete layer, the drop was about five times greater than the reported evaporation and for water levels within the aggregate layer the drop was about two-and-a-half times greater due to the material porosity, which was of 0.2 and 0.4, respectively.

Temperature and relative humidity were reported in degrees Celsius as a time series corresponding to each of the simulations.

Wind velocity was constant during the entire experiment, and reported in meters per second.

3.12 Parameterization

Evaporation is a complex process affected by many inter-related factors. As was described in Section 2.4, evaporation from shallow water bodies (potential evaporation) involves a series of parameters in which objective functions tie the variables together stochastically.

The parameterization of evaporation from pervious pavements, as applicable to the experiment design, included all factors relevant for open water bodies and additional parameters attributed to the porosity of the medium. Factors related to the scaling of the prototype were also included. At this point, the parameterization effort focused on identifying parameters in a descriptive manner based on common knowledge, experience and observation without providing functional relationships between them or identifying the sensitivity of a parameter. Some parameters were affected by other factors in the list, while other parameters were truly independent. Values of the parameters used during the

experiment are specified, where applicable. A compiled list of parameters for evaluation of the evaporation rates is presented in **Table 3.3**:

Table 3.3 List of parameters

No.	Para-meter name	Parameter description	Is this parameter dependent? (Y/N) *	List depen-dency	Values / Notes
1	W_T	Total weight of the apparatus	Y	All listed below	Primary dependent variable
2	Ta	Ambient air temperature	N	n/a	Controlled during the experiment
3	Ts	Surface temperature	Y	D_{LAMP}, P_{LAMP}, t_{SOLAR}	Controlled during the experiment
4	RH_a	Relative humidity – ambient	N	n/a	Controlled during the experiment
5	RH_s	Relative humidity – surface	Y	Ts, t_{SOLAR}	Was calibrated to mimic field behavior
6	dw_{ini}	Initial depth to water	N	n/a	Measured from the surface down. Controlled during the experiment
7	DIA	Inner diameter of the apparatus	N	n/a	4 inches (102 mm)
8	Hp	Pervious concrete section height	N	n/a	6 inches (152 mm)
9	D_{LAMP}	Distance from surface to the lamp	N	n/a	Controlled during the experiment
10	P_{LAMP}	Lamp power	N	n/a	125W or 250W.

					During the experiment set to 125W
11	S	Initial degree of saturation, for the material above ponded water surface	N	n/a	For the experiment, medium above water surface was wetted just prior to session start
12	k	Hydraulic conductivity	Y	n, ν	0.69 cm/s
13	n	Porosity	N	n/a	0.20
14	ν	Kinematic viscosity of water	N	n/a	Typical for tap water in room temperature
15	ρ	Density of water	N	n/a	Typical for tap water in room temperature
16	H_T	Total apparatus height	Y	H_P, H_B	42 inches (1067 mm)
17	H_B	Stone bed height	N	n/a	36 inches (914 mm)
18	H_P	Pervious concrete section height	N	n/a	6 inches (152 mm)
19	Td	Dew point	Y	Ta, RH	
20	e_0	Saturation vapor pressure at temperature of water surface	Y	RH, Ta, Td	
21	e_a	Vapor pressure of the air	Y	RH, Ta, Td	
22	u	Wind velocity near the surface	N	n/a	For the experiment, wind velocity was set to 1.66 m/s

23	t	Days since "rainstorm event"	N	n/a	
24	t_{SOLAR}	Solar time	N	n/a	Applicable to solar simulator performance

NOTES:

* Dependency of a parameter is defined here as whether it is affected by other(s) in this list.

Not all of those factors were incorporated into the experimental program due to the complexity of the problem. In lieu of performing a dimensional analysis using the entire range of parameters, the experiment focused on replicating typical field conditions and isolating one factor, initial depth to a water surface, which appeared as the most significant parameter. A regression analysis of the experimental data is described in Section 5.

4. Calibration

4.1 I-Buttons

Temperature readings from Thermochron and Hygrochron I-Button devices were checked for consistency. For this purpose, four devices (two of each type) were exposed to identical environmental conditions and the temperature data was recorded. The observed discrepancies were within ± 0.5 °C, which was consistent with the product specifications. It was concluded that such deviations were insignificant as applicable to the experimental settings.

Similarly, relative humidity readings from Hygrochron I-Button devices were checked for consistency. Two Hygrochrons were exposed to identical environmental conditions. The observed relative humidity discrepancies were within ± 5 % which was consistent with the product specifications. It was concluded that such deviations were insignificant as applicable to the experimental settings.

4.2 Thermocouples, thermocouple thermometer and thermocouple data logger

Thermocouples, a thermocouple thermometer, and a thermocouple data logger were calibrated at 100 °C using boiling tap water. The deviations were under ± 0.5 °C, which was within the specified equipment performance and acceptable for the purpose of the experiment.

4.3 Digital balance

The digital balances were checked for consistency using a stationary weight. A slight fluctuation of the reported weight with a clear cyclic behavior was observed. This phenomenon was attributed to ambient temperature fluctuations and its effect on the balance sensor. See **Figure 4.1** for the graphs correlating ambient temperature fluctuations (in °C) with the weight (in grams).

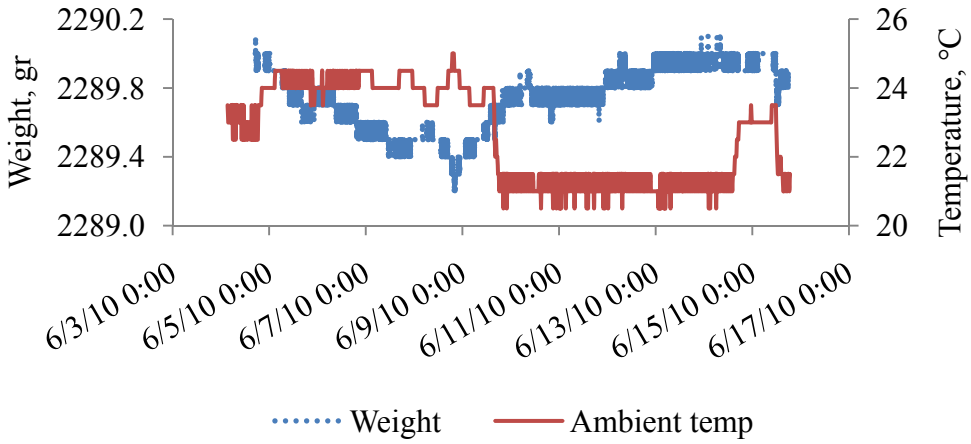

Figure 4.1 Balance accuracy

Although a very strong correlation between temperature and weight cycles was observed, the magnitude of the weight fluctuation was only 0.8 grams, which would translate into an evaporated water depth of 0.1 mm. Since the evaporation rates reported from the experiment data were in the order of 1 mm to 7 mm per day, the weight fluctuation was considered insignificant.

4.4 Wind speed

Calibration of the vane anemometer was performed using controllable air flow from the laboratory wind tunnel and a calibrated Pitot tube. The anemometer was positioned in front of the wind tunnel at a distance of 2 feet (0.61 meters). Four different air flow settings were used for development of the calibration curve, while recording wind velocity with both instruments – the anemometer and the Pitot tube. For each run, three Pitot tube measurements were taken just ahead of the stationary anemometer: at the top, center, and the bottom of the anemometer's front surface. The average reading was reported for the purpose of calibration curve construction. Pitot tube values were reported as head in inches of water. Bernoulli's equation was used to recalculate the head into velocity.

The anemometer velocity was recorded using 60 second time intervals measured with a stopwatch and reported in feet per minute. Refer to **Figure 4.2** for the constructed calibration curve.

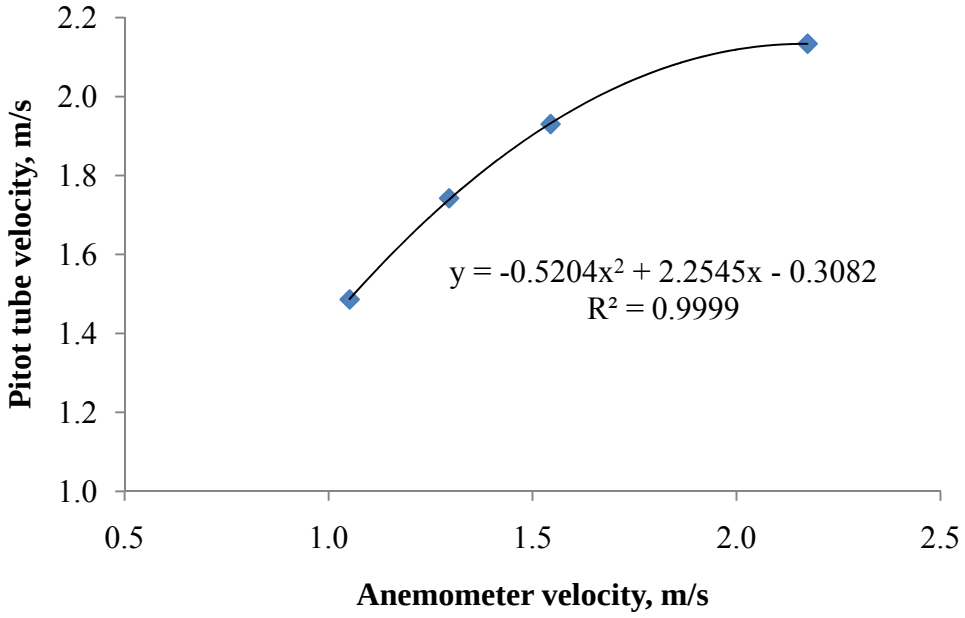

Figure 4.2 Vane anemometer calibration curve

The next step was to obtain the required wind speed for the experimental setup (on the order of 1.6 m/s). Since the lowest fan setting provided a velocity higher than the one required, a custom- made air gate was furnished to control the flow rate. The air gate was positioned just upstream of the fan to partially block the air intake. The air gate's area was experimentally adjusted until the near surface wind velocity was within the required limits (**Figure 3.27**).

The calibrated near surface wind velocity was 1.66 m/s (anemometer-measured uncalibrated velocity of 1.21 m/s). This value was representative of the average field condition observed at the Villanova pervious concrete SCM.

4.5 Solar simulator

The ultimate objective of the solar simulator calibration was to obtain induced heat characteristics similar to those exhibited by the sun. The prototype behavior was as recorded by a solar radiation sensor (Mendel Weather Station 2010) at the end of August 2010 at Villanova pervious concrete SCM. From observation of the solar radiation curve, energy delivered by the sun could be described by a truncated sine function. Immediately after sunrise energy output gradually increases, reaches its peak at solar noon, and then gradually decreases until sunset. The most direct way to mimic such behavior was by utilizing a heat source with a programmable variable power output. However, a gradually variable power output option was prohibitively complex; therefore it was decided to use the pulse modulation principle to obtain the desired characteristics. A simplified conceptual diagram showing the pulse modulation principle was presented earlier in **Figure 3.29**.

The collected data proved that, as hypothesized, delivering a given amount of energy in discrete pulses produces a temperature response similar to the scenario with energy delivered in a continuously variable manner. This approach worked because the experimental setup exhibited thermal inertia: with the pulse cycle set at a sufficiently short duration, the temperature response became not discrete but continuous.

Two calibration parameters were considered: the duration of the pulse cycle and the methodology for correlation of the daily solar radiation to the pulse duration. The pulse cycle was defined by a fixed total duration, D_{TOT}, and comprised of continuously variable durations of power on and power off, D_{ON} and D_{OFF} respectively. Therefore, at any given time, the pulse cycle duration could be described as following:

Equation 4.1 Pulse cycle duration

$$D_{TOT} = D_{ON} + D_{OFF} = \text{Constant, where}$$

D_{TOT} = total pulse cycle duration, in minutes,
D_{ON} is pulse duration, in minutes,
D_{OFF} is pulse delay, in minutes

The pulse duration and pulse delay were assigned using the reference solar radiation information obtained from the Villanova pervious concrete SCM site. The following principle was employed: the pulse duration fraction was set to be equal to the solar radiation fraction, as described by the following formula:

Equation 4.2 Pulse duration fraction

$$D_{ON} / D_{OFF} = Rad_{MAX} / Rad_0 \text{ , where}$$

D_{ON} , D_{OFF} as previously defined,
Rad_{MAX} = maximum solar radiation during one daily cycle,
Rad_0 =instantaneous solar radiation corresponding to a given time,

A regression analysis was performed to express the instantaneous solar radiation mathematically. The following relationship describes the behavior with the coefficient of determination, $R^2 = 0.9991$:

Equation 4.3 Instantaneous solar radiation

$$Rad_0 = a * \sin(2 * \pi * b * T + c) + |a * \sin(2 * \pi * b * T + c)|, \text{ where}$$

Rad_0 = as previously defined,

T = time of the day, in days,

a = 373.084 (regression coefficient),

b = -0.906 (regression coefficient),

c = 4.664 (regression coefficient),

π is expressed in radians

Using the aforementioned expressions, the start of the pulse delivery (at sunrise), pulse modulation during the day, and pulse termination (at sunset) were defined and tied to the time of the day and corresponding solar radiation. After several calibration iterations, a duration of one pulse cycle, D_{TOT}, was set to 0.625 minutes (37.5 seconds).

Since no direct feedback loop was built into the solar system, the ultimate check of the solar simulator performance was done by assessment of the resulting thermal behavior, which is described in detail Section 4.6.

4.6 Thermal response

As discussed in Section 3.5, the temperature behavior of pervious pavement systems is subjected to seasonal and daily patterns. The temperature variation throughout a pervious pavement system (thermal profile) is affected by a number of factors, such as the solar radiation and thermal conductivity of the medium. Surface and near-surface layers exhibit a high response to solar radiation varying seasonally and daily. This response decays and eventually becomes extinct as the depth from the surface increases. As demonstrated by one study, summer-time daily temperature fluctuations extend to a depth of about 28 inches (711 mm) (Kevern et al. 2009), creating a highly dynamic temperature conditions.

To achieve the objectives of the experiment, it was desired to re-create a thermal profile representative for the Villanova University pervious concrete system during a typical summer day. Solar and temperature conditions recorded at the VU pervious concrete site at the end of August 2010 were used for calibration of the experimental setup. The first boundary condition of the target thermal profile was defined by the surface temperature

measured with I-Button Thermochron data logger positioned directly on the pavement surface. Second boundary condition was defined by the aggregate bed temperature recorded at a depth of 40 inches (1016 mm) with INW PT2X pressure/temperature data loggers. Solar radiation measurements, in watts/m^2, were obtained from the Villanova University weather station maintained by the Department of Astronomy (Mendel Weather Station 2010).

To eliminate interference with other environmental factors such as rain and clouds, temperature and solar radiation data used for the calibration were selected from a period characterized by three consecutive clear days: August 27 through August 30, 2010. The obtained temperature data was within the typical range for late August. **Figure 4.3** is a composite graph of the boundary temperature conditions and the corresponding solar radiation.

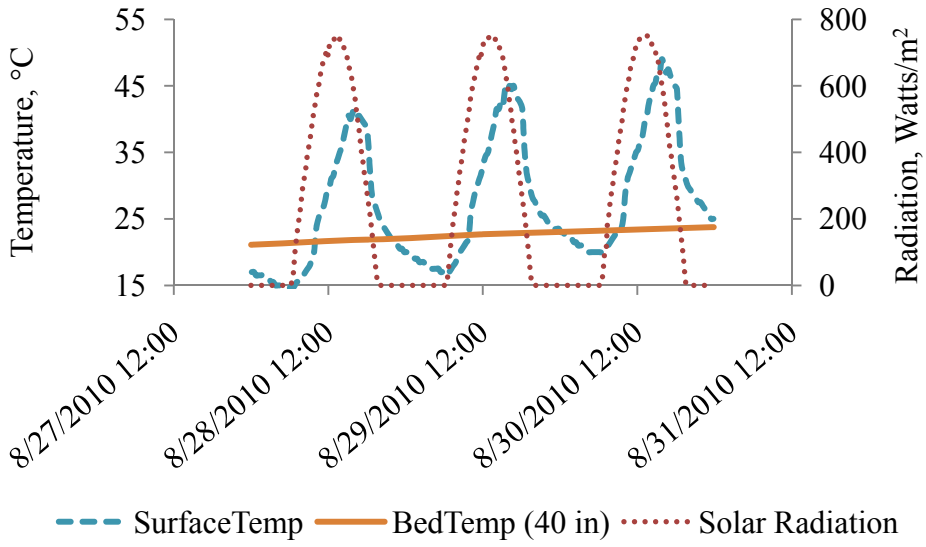

Figure 4.3 Target thermal profile: boundary conditions, VU pervious concrete SCM

Among the calibration parameters available to approximate the simulated behavior to the one observed in the field were variable intensity of the heat source (solar simulator), power setting of the heat source, distance from the heat source to the pervious concrete surface and ambient conditions in the laboratory. The optimized parameters were: solar

simulator intensity was as described in Section 4.5, power output of the lamp was set to 125 Watts, distance from the heat source to the pervious concrete surface was 3.5 inches (89 mm), and ambient temperature was 21° C. With all aforementioned parameters optimized, a temperature response of the experimental apparatus was achieved (**Figure 4.4).** In this figure, the time-dependent heat source intensity is denoted as a fraction of the maximum radiation (applied at solar noon).

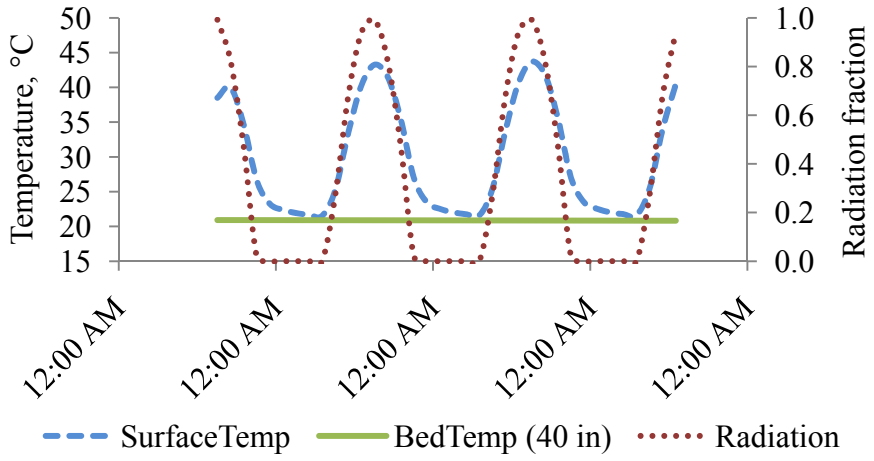

Figure 4.4 Thermal profile: experimental apparatus

As observed from **Figure 4.4**, the boundary conditions match closely, but not perfectly. Several aspects were given detailed consideration; among them were the general shape of the surface temperature response, temperature amplitudes, and temperature trends.

As observed in **Figure 4.3**, which depicts the field conditions, the surface temperature curve is not smooth, particularly, in the upward ramp where several sharp turns are observed. Additionally, the slope of the upward ramp was not as steep as in the corresponding segment of the experimental data (**Figure 4.4**). This temperature response of the surface layer was due to obstructions (adjacent buildings) that created shading conditions. To assess the extent of the shading, a site solar survey was performed. Solar altitudes of the obstructions corresponding to the incremental solar azimuths were recorded and measured at the location of temperature sensor installation. The obtained data was superimposed onto a solar paths diagram corresponding to the latitude of 40°

North, which corresponds to the approximate site latitude. **Figure 4.5** provides the details of the site shading diagram.

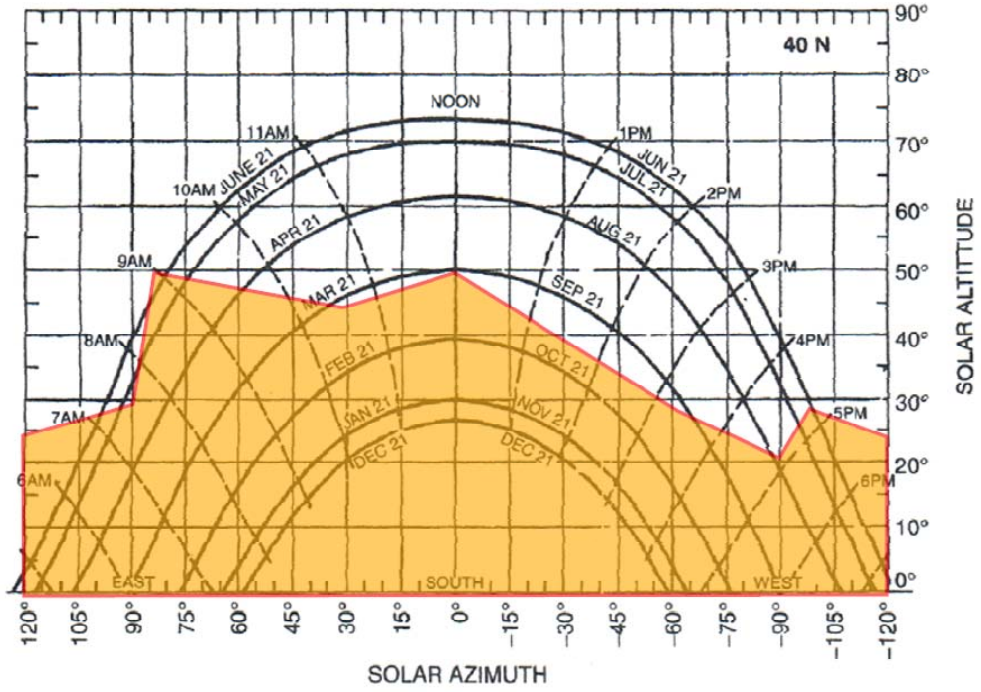

Figure 4.5 Site shading diagram

The solar path of August 21, as indicated on the diagram, was the closest one to the observation period. The shaded polygon area represents the times of the day when the surface does not receive direct sunlight due to obstructions. From the diagram interpretation it follows that the surface was shaded from sunrise to about 9:30 AM, was clear from 9:30 AM to about 4:45 PM, and was shaded again from 4:45 PM through sunset. This explains the irregularities in the surface temperature response, a more gradual slope of the upward ramp, and also indicates that the site does not receive the maximum possible solar radiation.

For the calibration purposes, the shading-related temperature irregularities observed in the field, were not replicated. Therefore, the temperature response created in the experimental setup was representative of a surface completely exposed (non-shaded) during the entire day.

The next aspect requiring clarification was temperature trends that extended beyond 24 hours. As could be observed from the field data (**Figure 4.3**), the surface and 40 inch (1016 mm) temperatures grow over the period of three days, whereas the experimental data (**Figure 4.4**) does not exhibit such trends. This discrepancy could be explained by looking at the environmental conditions that preceded the observed period. The Villanova SCM site experienced colder weather just prior to the observation period while the experimental setup was subjected to constant temperature conditions for over one week. Therefore, at the time of data collection, the experimental setup was at thermal equilibrium while the SCM was not.

Lastly, the surface temperature daily minimums observed at the site were slightly lower than the surface daily minimums of the experimental apparatus. This was due to the limitations of the experiment design, however, given the magnitude of the deviation, this aspect was considered insignificant.

In addition to the boundary conditions, the temperature behavior in the intermediate depth layers (from the surface to 40 inches (1016 mm) deep) was also evaluated in the calibration stage. Since data from the prototype site for the intermediate layers was not available, it was obtained from an independent temperature behavior study (Kevern et al. 2009). This year-long investigation reported a temperature profile of a pervious concrete system at Iowa State University at a depth of 3 inches (76 mm) through 64 inches (1626 mm). Analysis of this data revealed that the zone of daily temperature fluctuation extended to a depth of about 28 inches (711 mm) below the surface while temperature changes in deeper layers were evident only on a seasonal scale. This condition was satisfied in the calibrated experimental apparatus performance: in thermal equilibrium conditions, daily temperature changes in the experimental apparatus were evident only at depths higher than 28 inches (711 mm). **Figure 4.6** presents a typical three-day calibrated thermal profile achieved in equilibrium conditions.

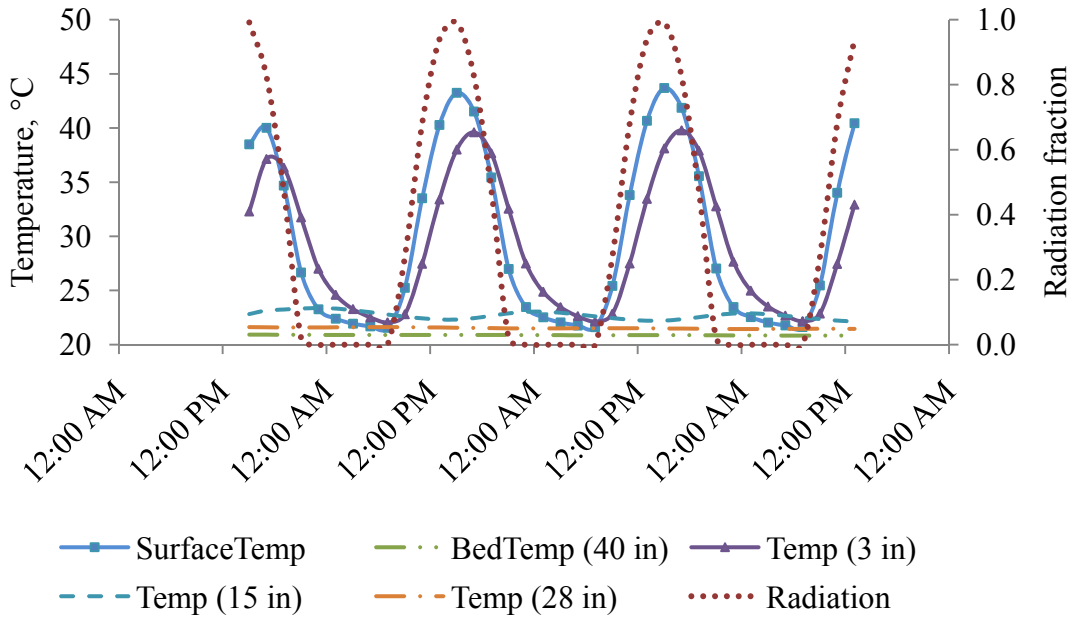

Figure 4.6 Experimental apparatus: typical thermal profile

In general, weather patterns are much more dynamic and complex than the controlled environmental conditions in the laboratory; therefore, direct replication is not always feasible. However, approximation of the environmental conditions is sufficient to simulate the desired behavior. Overall, it was concluded that the temperature behavior typical for the Villanova pervious concrete system in late August was successfully replicated in the experimental setup.

4.7 Relative humidity

The objective of the relative humidity calibration was to have the laboratory behavior replicate the field behavior. The field relative humidity during three days in late August 2010 was recorded by and obtained from the Villanova University weather station (Mendel Weather Station 2010). The behavior exhibited a cyclic pattern as shown in **Figure 4.7**.

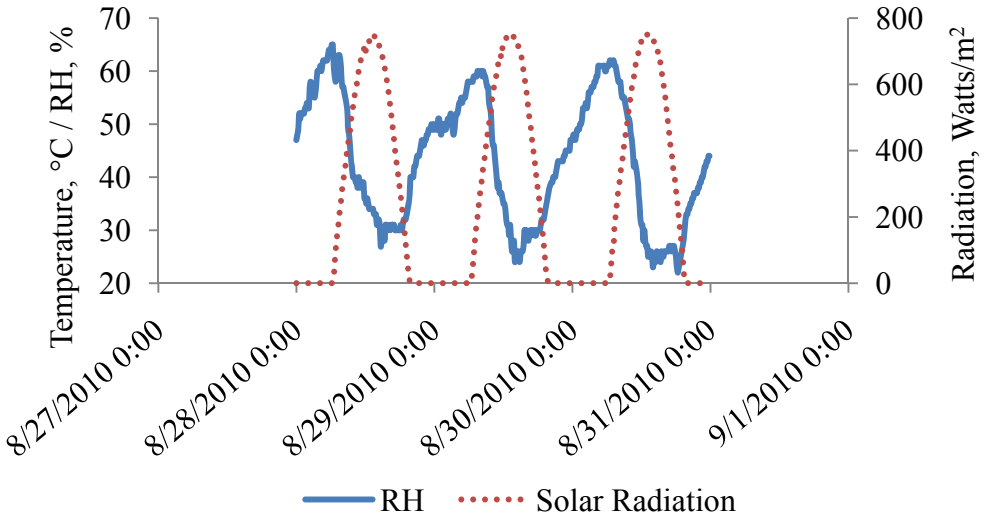

Figure 4.7 Field relative humidity

The ambient relative humidity and the distance from the "artificial sun" to the pervious concrete surface were the calibration parameters used to obtain similar behavior in the laboratory settings. The latter parameter was constrained since it also served for calibration of the temperature response (Section 4.6).

As became evident during calibration, a local microclimate was established near the pervious concrete surface: the relative humidity responded to the artificial sun in a way similar to field behavior, even though the ambient relative humidity in the environmental chamber remained constant. This phenomenon eliminated the need for a programmable relative humidity controller and significantly simplified the calibration procedure, which was reduced to setting the ambient relative humidity to a constant value.

The optimization of the parameters resulted in an ambient relative humidity of 50% and the distance from the heat source equal to 3.5 inches (89 mm). The simulated relative humidity typical for all experimental runs is shown as **Figure 4.8**.

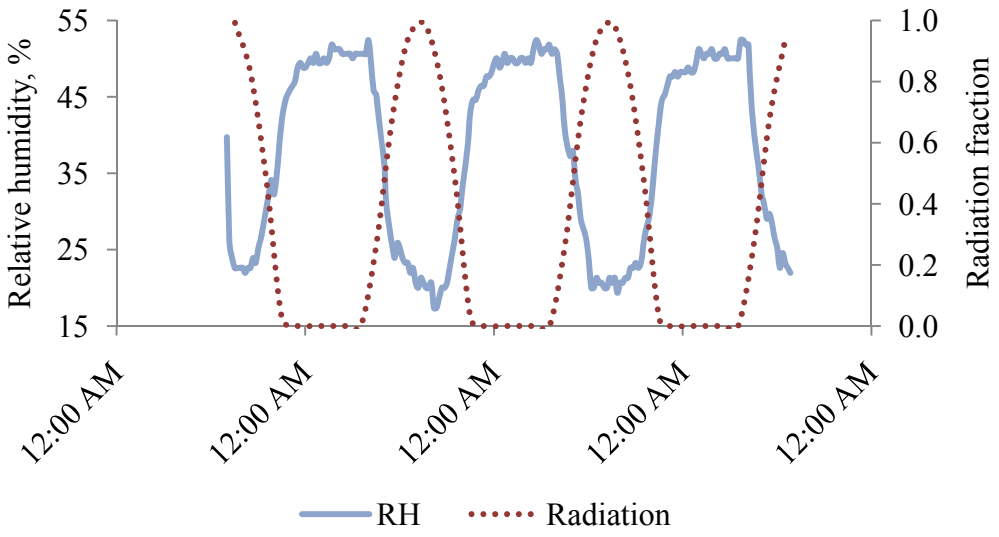

Figure 4.8 Simulated relative humidity

As can be observed by inspection, the cyclic behavior of the relative humidity and the amplitude were matched sufficiently closely. The field behavior exhibited more pronounced peaks in relative humidity values while the simulated conditions showed plateau segments, especially during the night time. This difference is thought to be due to lesser stored heat capacity of the experimental apparatus because of its small footprint.

Overall, it was concluded that the relative humidity behavior was replicated successfully.

5. Data and results

Data was collected according to the experimental program described in Section 3.11. Six simulation runs were performed, each having a different initial depth to the ponded water surface. One of the runs was incomplete due to equipment failure: its duration was 48 hours instead of 72 hours as designed. The remaining five runs had complete datasets.

5.1 Collected data

Each simulation run generated session data consisting of the total weight of the apparatus, the thermal profile data, the ambient and surface relative humidity, and the ambient temperature. Each dataset consisted of a time series with data taken at specified intervals.

The thermal profile data was taken in one minute intervals, the surface and ambient relative humidity and ambient temperature were taken at 20 minutes intervals, and the weight data was taken every 5.3 seconds – the maximum delay allowed by the scale settings. The solar time for each session (the time used by the solar simulator) was also reported. Since the experiment was conducted indoors, the simulator solar time did not have to correspond to the actual time of the day (system time reported by the computer). For the purposes of convenience, the solar time was shifted by minus 1.5 hours from system time for the duration of the experiment.

Upon completion of a simulation run, the dataset was imported into a spreadsheet (Microsoft 2007) for processing. The weight data typically consisted of 49,020 records, thermal profile data - of 4,324 records, while surface and ambient relative humidity and ambient temperature consisted of 218 records for each dataset.

5.2 Data processing

An overview of the raw weight time series revealed that some level of noise was present throughout each of the simulation runs. The noise originated from the design of the experiment: the apparatus, which had a shape of a slender column, exhibited slight side sway in response to the wind blowing over its surface. The balance supporting the column was sensitive enough to respond to this sway action, resulting in a recorded weight fluctuation with an amplitude of about 2 grams. The weight readout fluctuated up and down; therefore, averaging the values over an appropriate time period would have solved the noise problem. A two and a half minute period was chosen for the averaging process. Since the data was collected at a very fine interval (5.3 seconds), averaging it over the specified interval did not reduce the amount of usable data because two and a half minutes was still a sufficiently fine increment to preserve evaporation trends.

The simulations ran back to back starting at 12:30 PM solar time and lasted 72 hours. Approximately 10 minutes was required to initialize each run, therefore the actual duration of each run was about 71 hours 50 minutes. Since 72 hours of data was required for the analysis, the weight time series for the last 10 minutes of each run were linearly

extrapolated. This projection was very small compared to the amount of actual data: about 23/100 of one percent. The evaporation was calculated from the loss of mass in the system and reported in equivalent vapor loss in an open water body in millimeters of water. The following equation was developed to convert the weight loss into evaporation:

Equation 5.1 Weight to evaporation conversion

$$E = \Delta W_T / (A * 1x10^{-3} * \rho), \text{ where}$$

E = evaporation, as defined above, in mm

ΔW_T = change in weight of the system, in grams

A = net cross-sectional area of the pervious concrete specimen, in m^2

ρ = density of tap water at 20 °C, in kg/m^3

The evaporation rates were calculated as a first derivative of the evaporation data. A typical complete dataset from one simulation run is presented in **Figure 5.1** with a discretization time step of 30 minutes. This simulation run had an initial depth to the ponded water surface equal to zero inches (zero mm).

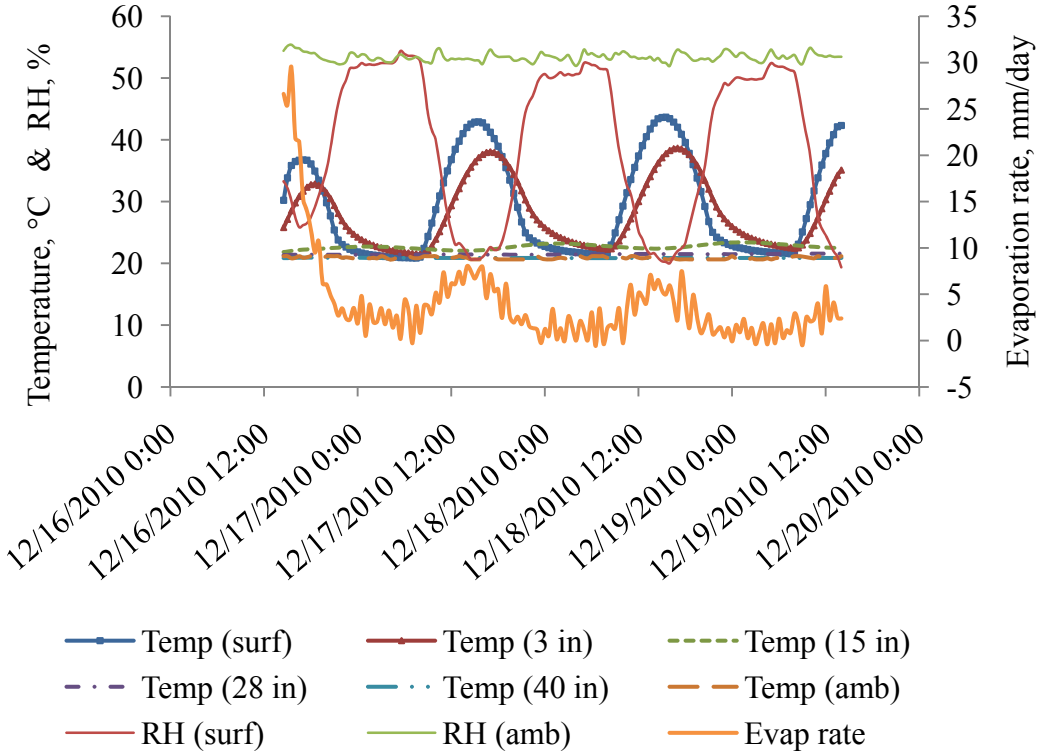

Figure 5.1 Typical dataset

As could be observed from the presented data, cyclic trends due to daily variable solar simulator output are evident in the thermal profile formation, relative humidity and evaporation rates.

Prior to analyzing the experimental data, it was necessary to perform data integration. Integration was performed to translate the time series into a format that evaporation is typically reported in (i.e. 24-hour base). All data within a 24 hour period was averaged. Since the duration of each simulation run was 72 hours (three days), the integration procedure reduced each dataset to three data points. Evaporation rates were presented in mm/day and the time reported as hours elapsed since the simulated rainstorm event.

The resulting 24 hour evaporation datasets from all six simulations are presented in **Figure 5.3** and **Figure 5.3**, showing cumulative evaporation and evaporation rates respectively.

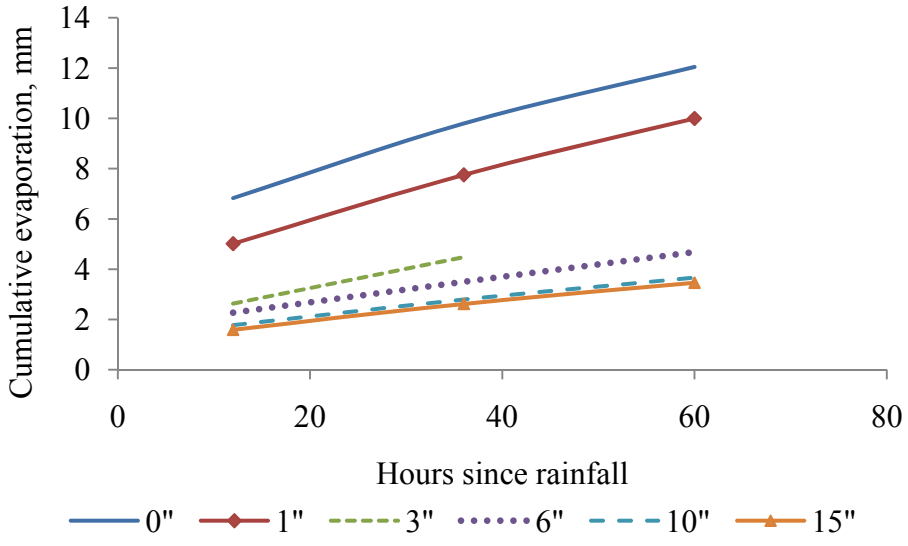

Figure 5.2 24-hour cumulative evaporation datasets

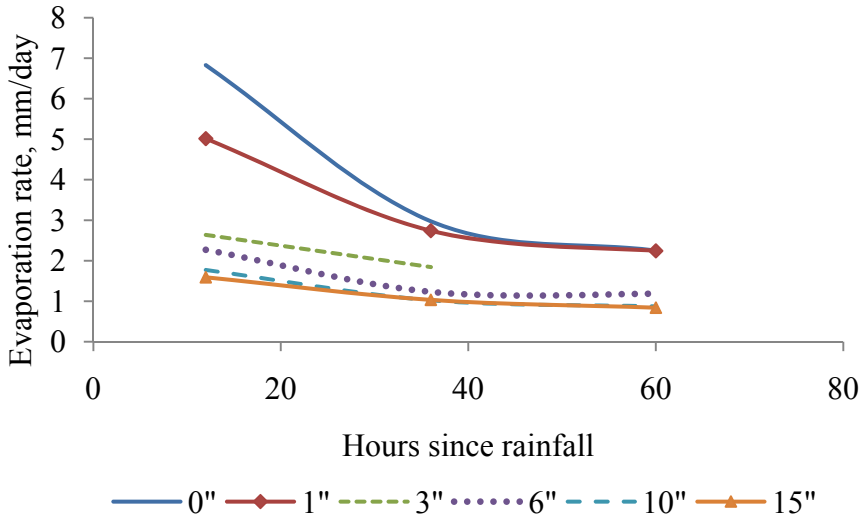

Figure 5.3 24-hour evaporation rate datasets

Although 24-hours is the typical reported format for the evaporation rates, it does not preserve the evaporation behavior that occurs within a 24 hour period in response to changing radiation conditions. To demonstrate the daily response in evaporation behavior, another dataset was created with the integration interval of 2 hours. Integrating was performed to eliminate the noise in the calculated evaporation rates that were shown in **Figure 5.1**. The resulting 2-hour evaporation datasets presented in **Figure 5.4** and **Figure 5.5**, show the cumulative evaporation and the evaporation rates respectively. Refer to **APPENDIX D** for a complete data from each 2-hour dataset.

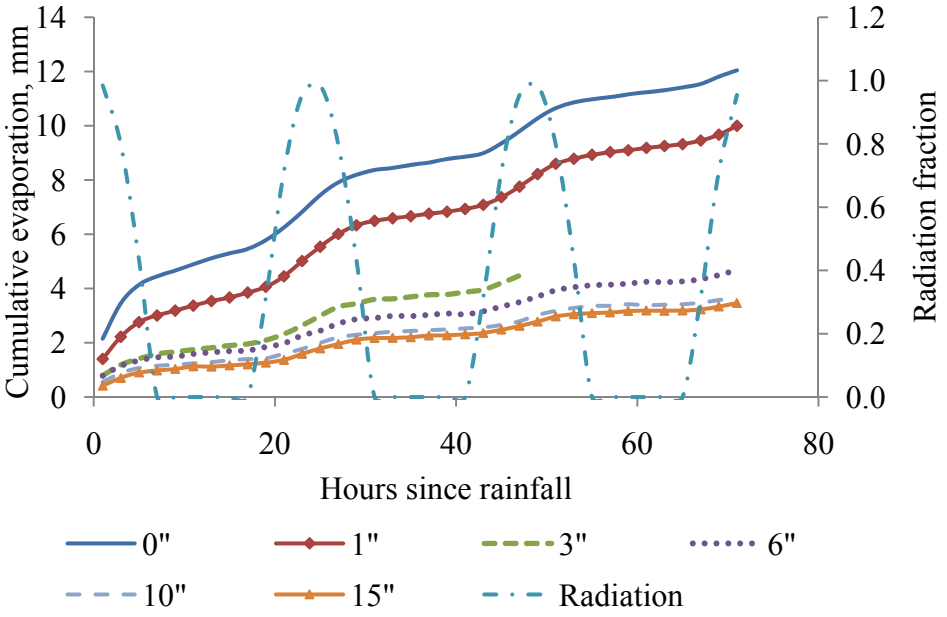

Figure 5.4 2-hour cumulative evaporation datasets

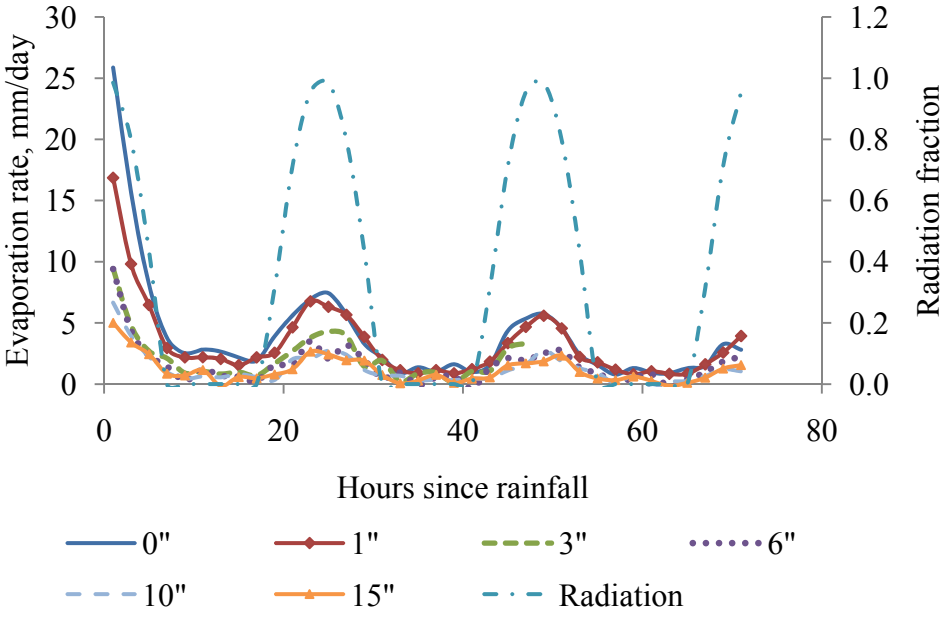

Figure 5.5 2-hour evaporation rate datasets

As per experiment program, the duration of each of the simulation runs was 72 hours (three days). Limitations to the experiment run time did not allow for longer individual sessions. However, the last simulation (initial depth to water surface equal to 15" (381 mm)) was allowed to run for 264 hours (11 days) to investigate the affects of longer durations. Similarly to the datasets described above, this simulation was integrated using a 24 hour time step and 2 hour time step. **Figure 5.6** and **Figure 5.7** present the 24-hour cumulative evaporation and the evaporation rates respectively.

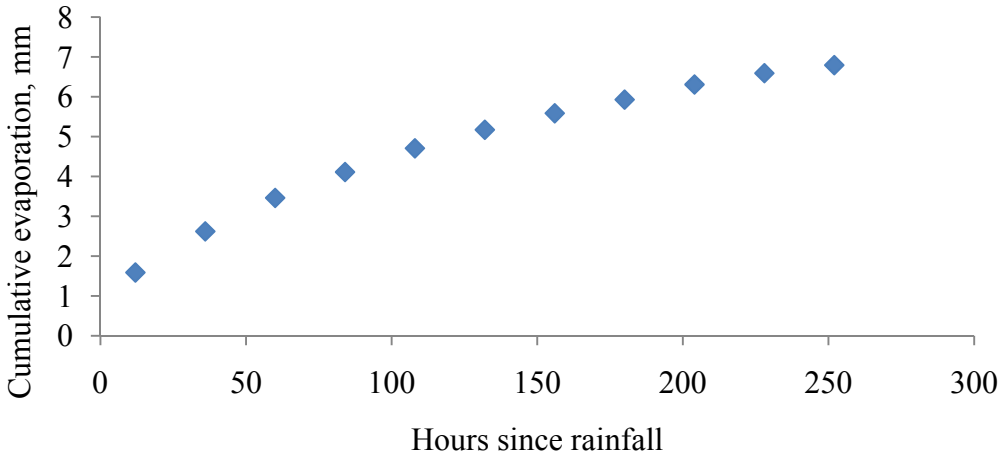

Figure 5.6 24-hour cumulative evaporation, 11 days, d=15"(381 mm)

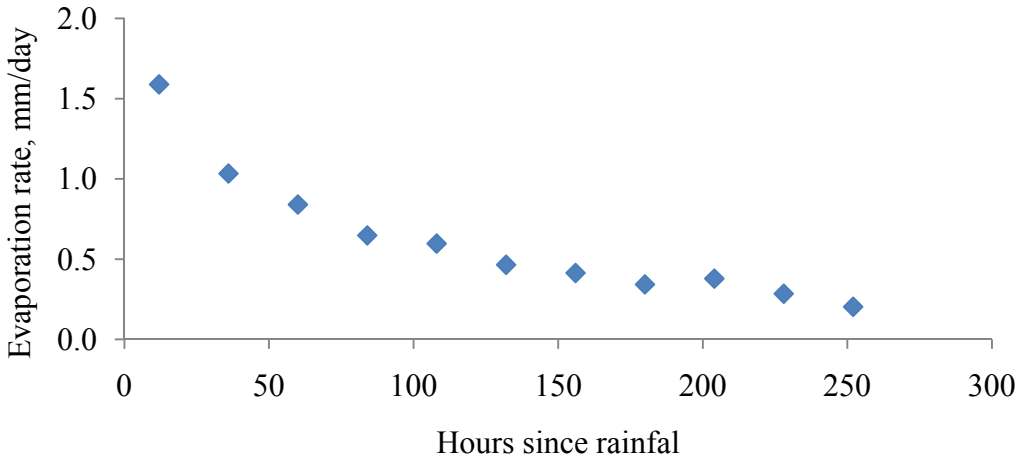

Figure 5.7 24-hour evaporation rate, 11 days, d=15"(381 mm)

Figure 5.8 and **Figure 5.9** present the 2-hour cumulative evaporation and the evaporation rates respectively.

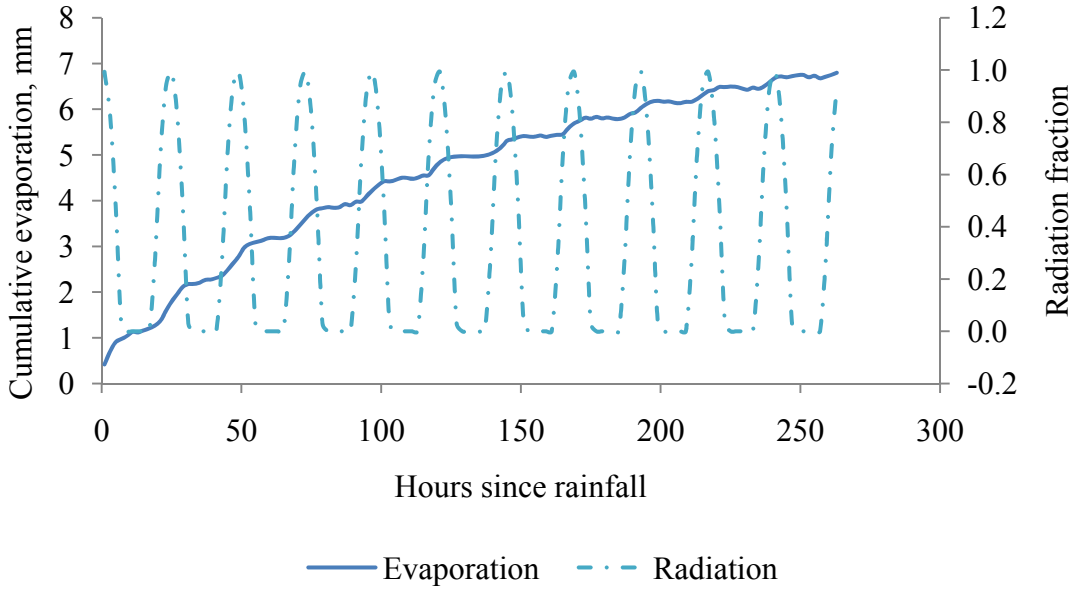

Figure 5.8 2-hour cumulative evaporation, 11 days, d=15”(381 mm)

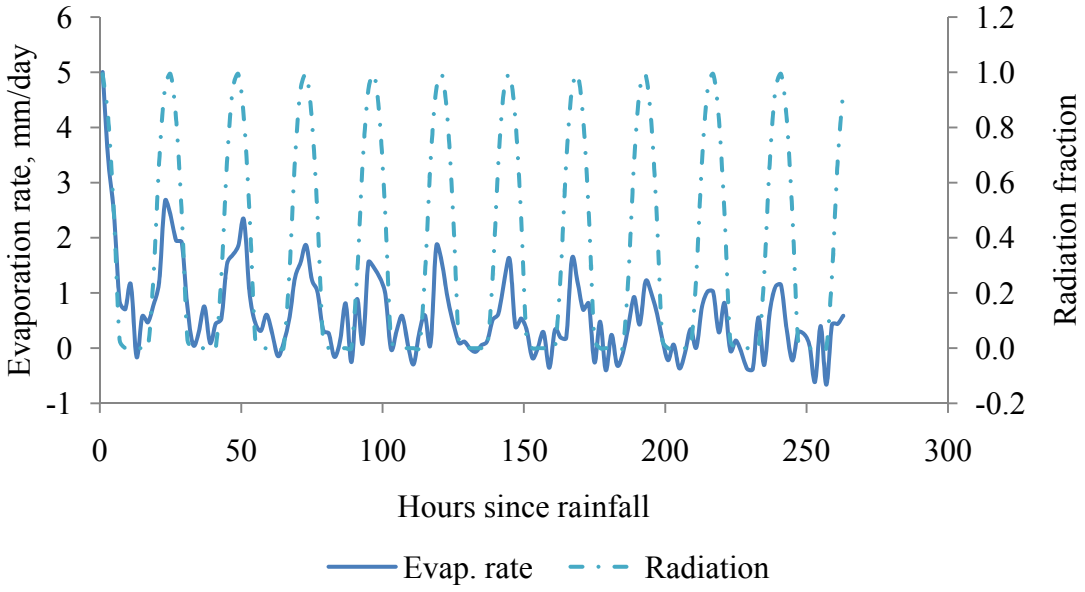

Figure 5.9 2-hour evaporation rates, 11 days, d=15”(381 mm)

5.3 Data analysis

The processed 24-hour data was analyzed to find a potential predictive relationship characterizing the evaporation behavior. Two technical computing tools were used for the regression analysis: Matlab R2010a and SPSS 16.0.

It was hypothesized that the evaporation behavior observed during the experiment could be described analytically in terms of two independent variables: time that had elapsed since the "rainfall event" and the initial depth to a ponded water surface. Using six datasets integrated over a 24-hour period, the data was graphically presented as evaporation rate (EVAP, in mm/day) vs. initial depth (D, in mm) vs. time (T, in hours). The resulting data points are presented in **Figure 5.10**.

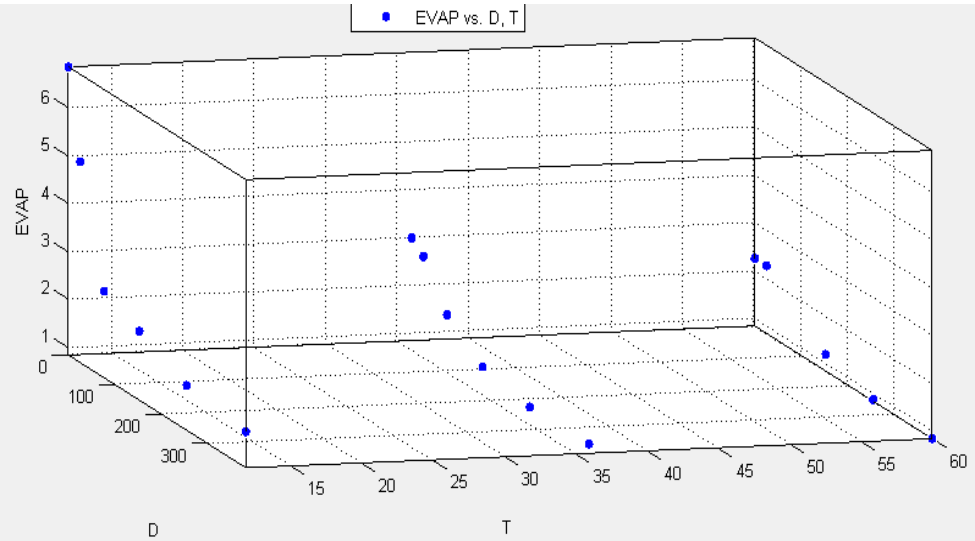

Figure 5.10 Actual evaporation rate vs. initial depth vs. time

Multiple regression analyses were performed to identify the objective function that would match these data. The best relationship satisfying the data requirements was of the following form:

Equation 5.2 Daily evaporation rates

$$EVAP=a*[(D/25.4+1.5)*T-b]^{c}+d, \text{ where:}$$

EVAP = evaporation rate, in mm/day

D = initial depth to a ponded water surface, in mm

T = time, in hours, since the end of the rain event; {T ≥ 12 hrs}

a = 33.36 (regression coefficient),

b = 5.24 (regression coefficient),

c = -0.647 (regression coefficient),

d = 0.47 (regression coefficient),

For this relationship, the coefficient of determination, R^2 was equal to 0.9774 (adjusted R^2 = 0.9722), which indicated a sufficiently close match of the experimental data to the objective function.

The surface created from **Equation 5.2** was plotted and compared with the experiment data. **Figure 5.11** and **Figure 5.12** present the predicted surface and the residuals, respectively. The low residual values and high R^2 value indicates that the proposed relationship fits the data reasonably well.

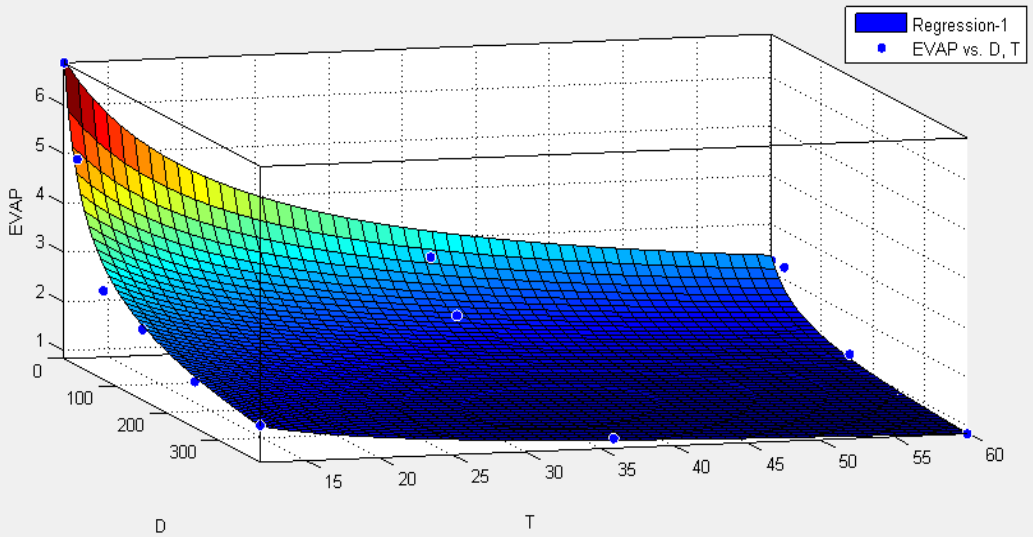

Figure 5.11 Predicted evaporation rate vs. initial depth vs. time

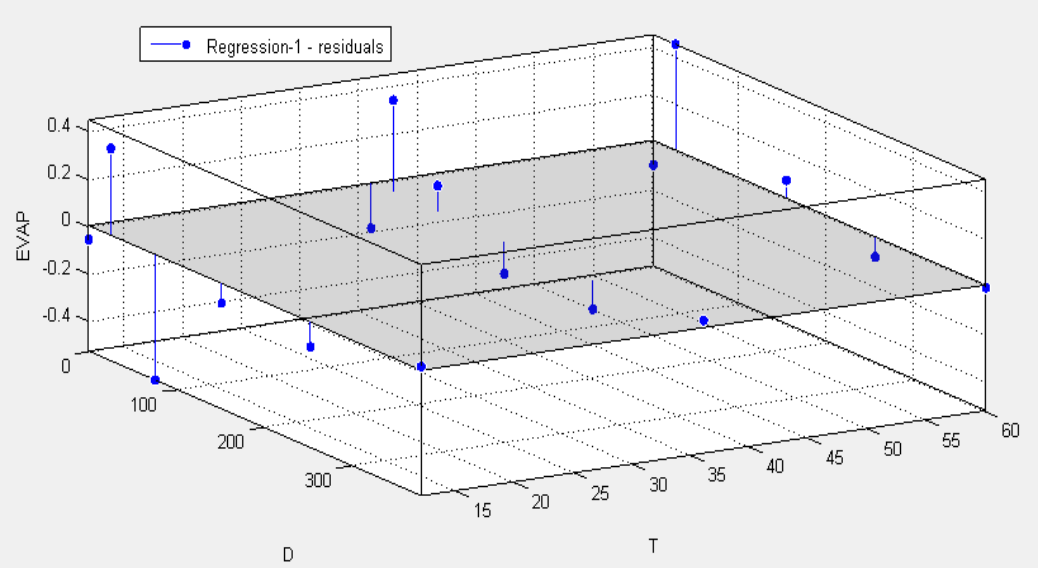

Figure 5.12 Residuals

5.4 Validation of the results

Since the evaporation behavior of pervious pavements has not been extensively studied, no data for direct comparison was available to validate the experiment results. However, it was possible to perform an order of magnitude validation using compiled meteorological data and the results available from published literature. Boundary conditions were used for such assessment: a simulation initially at saturation and a simulation with the water level below the influence zone. They were compared, respectively, with a surface evaporation and the evaporation from another pervious pavement system which utilized an underdrain.

5.4.1 Saturated initial conditions

The average daily free water surface evaporation for the month of August in the vicinity of Villanova, PA is approximately 5.4 mm/day (calculated using data from NOAA TR-33, 1982 and NOAA TR-34, 1982). Compared with this estimate, the 24-hour evaporation rate observed for the simulation with initially saturated conditions (water surface flush with concrete surface) was 6.83 mm/day, which is 26% higher. Obviously,

such a comparison is not performed on a one-per-one basis, although it might provide a quantitative description of the evaporation process.

Several possibilities for the discrepancy in the evaporation rates were considered. One possible explanation is that the surface layers of the pervious concrete system are significantly hotter than the free water surface during the same conditions (due to different surface reflectivity and other factors). Another explanation could be that the observed experimental results are unrepresentatively high because the simulations were modeled after a pervious concrete system performance on a cloudless day, and not after a day with an average sky cover conditions. Since there is no compatible reference data to validate the experimental results, having a free water surface evaporation within 26% of saturated conditions was found sufficient for an order of magnitude validation.

5.4.2 Initial water level below influence zone

Another attempt to validate the results was done by comparing the experiment data with the results of a full scale field evaporation study performed at University of Muenster, Germany (Starke, Göbel and Coldewey 2010). As discussed in Section 2.5, the pervious pavement system in this study consisted of water permeable concrete paving stones with pervious seams. The physical properties of those materials were not analogous to those of pervious concrete. The reported hydraulic conductivity was 8.1×10^{-4} m/s for the stone and 3.3×10^{-3} m/s for the seams, which were significantly lower than the 7.4×10^{-3} m/s for the pervious concrete used in the experimental apparatus (see Section 3.2). Additionally, the German experimental setup utilized an underdrain that did not allow ponding of the water, therefore comparison was limited to the simulations with ponded water surface lower than the influence depth (see Section 5.5.1). The maximum daily evaporation rates for the month of August from the experiment at the University of Muenster were about 0.6 mm/day and recorded within 24 hours of a rainstorm event. In contrast, the maximum evaporation rate obtained from the laboratory simulation with the initial depth to water surface of 15” (381 mm) were over 2.5 times greater and amounted to 1.6 mm/day, also recorded within 24 hours of a simulated rain. Such a discrepancy is most likely due to differences in hydraulic conductivity; however, pavement temperature

conditions (not reported in the Muenster study) might have also contributed. Even though direct validation of the experiment results was not possible, an order of magnitude check was satisfactory and the simulated evaporation rates were expected to be greater than those observed at the University of Muenster due to differences in hydraulic conductivity.

5.5 Data interpretation

5.5.1 The evaporation behavior

The relationship of the hydrologic response of the pervious concrete system to the mechanisms of evaporation was briefly discussed in Section 3.6. It was hypothesized that the vapor transfer mechanisms include evaporation from the water surface and the evaporation from the medium above the water surface (applicable in unsaturated conditions only). The latter may include inter-particle voids containing trapped water that was unable to infiltrate and, to a lesser extent, water adsorbed to the surface of the particles.

The experiment data showed that evaporation correlates very strongly with the intensity of solar radiation during the daily cycle. As could be observed from **Figure 5.5**, maximum evaporation rates coincide with the maximum radiation which occurs at solar noon.

The observed peaks in the surface temperature also coincided with the peaks in radiation (see **Figure 4.6** for details). On the other hand, peaks in sub-surface temperatures were observed to lag behind peaks in radiation – a phenomenon that could be attributed to the thermal inertia of the medium. The thermal inertia could be described as a time delay in the heat wave propagation as it travels through the medium. It was observed that as depth to the point of measurement increases, so does the time lag from solar noon to the temperature peak. This phenomenon was also observed in a different study that monitored field conditions as shown in **Figure 3.10** (Kevern et al. 2009).

Temperature is the primary driving force affecting the intensity of water vapor transfer (see Section 2.4). Since the timing pattern of the observed evaporation rates followed the

timing established by surface temperatures (and not sub-surface temperatures), it could indicate that the bulk of the vapor transfer occurs from the surface layers, regardless of the evaporation mechanism.

The initial depth to the ponded water surface was found to correlate very strongly with the daily evaporation amount. The period for cyclic behavior of the evaporation rates was not affected, but the amplitude diminished exponentially as the initial depth to water surface increased (see **Figure 5.4**).

The evidence obtained in the experiment supports the hypothesis that evaporation from the ponded water surface plays a major but not exclusive role, and is particularly important when the water table is very near the concrete surface. As the initial depth to ponded water increases, the evaporation rates drop dramatically, but not to extinction, and eventually become unaffected by the additional increase in depth. An insignificant change in the evaporation rates with initial depth to water surface of 10 inches (254 mm) compared to 15 inches (381 mm) suggests that evaporation from the water surface did not contribute to water vapor transfer in those simulations.

The observed evaporation behavior suggests that an influence zone exists within which the water surface contributes toward total evaporation, and beyond which evaporation rates are not affected by the water surface elevation. Based on the experiment data, it was concluded that the lower limit of such influence zone is approximately 10 inches (254 mm) below concrete surface. This finding is important for optimizing the design of pervious concrete structures for maximum evaporation.

The time elapsed since the end of a simulated rainstorm event exhibited a strong correlation with the daily evaporation rates. The retreating water surface and finite availability of water trapped in the inter-connected void spaces explain the drop in evaporation rates as time progresses. The daily evaporation rates continued to decline gradually after three days of monitoring, as could be observed from the last simulation, which was allowed to run for 11 continuous days (**Figure 5.6**).

5.5.2 Hydrologic perspective

Unsaturated conditions produced much smaller evaporation rates as compared to the simulations with the initially saturated medium. Even though unsaturated conditions are expected to prevail in a typical BMP operation, evaporation could still play a measurable role in the yearly water budget – especially if the BMP is designed to promote evaporation. This section will concentrate on the evidence supporting the latter statement in light of the experiment results.

It is important to emphasize that the experiment modeled the performance of a hypothetical pervious pavement SCM –one with the inhibited infiltration. Most pervious pavement SCMs in use today are required to utilize infiltration or other means of stored runoff release, such as an underdrain. For example, the state of Pennsylvania sets infiltration rates of 0.1 inches/hour (2.5 mm/hour) as a minimum requirement for the applicability of pervious pavements with infiltration beds, however, design reduction coefficients and factors of safety are likely to increase this estimate by a factor of 2 to 10 (PADEP 2006). Therefore, the performance of such a hypothetical BMP cannot be directly related to the ones currently in use, although some estimates could be made for indirect comparison. At a minimum, the evaporation behavior in the field is expected to correspond to a simulated scenario with the water level below the influence zone. The actual evaporation rates would depend on the infiltration or outflow rates and the initial depth to the water surface, and is expected to be within the bounds established by the saturated and low water level conditions.

A detailed assessment of the results of this experiment on the scale of a SCM's hydrologic performance would require substantially more experimental data and intensive modeling. Since the availability of such data was beyond the scope of this experiment, basic assumptions and simple calculations were utilized to perform an order of magnitude assessment of a SCM with inhibited infiltration. The annual evaporation from the pervious concrete system was projected using the available data on free water surface evaporation. The main assumption was that the pervious pavement evaporation distribution throughout the year follows that of a free water surface. Meteorological

assumptions were based on several years of weather pattern observations at Villanova University and included five rainstorm events per month on average. Further, it was assumed that no additional evaporation occurs after the first three days following the end of a rainstorm. This assumption was rather conservative because the evaporation process, although slowing down, continues well past the first three days, as was demonstrated in one of the simulation runs. This contingency was justified to compensate for a possible overestimation because of the clear sky assumption: as mentioned previously, the experiment did not account for the sky cover and the shading.

The average annual free water surface evaporation in Philadelphia, PA is 35 inches (889 mm) (NOAA TR-33, 1982 and NOAA TR-34, 1982). The monthly evaporation distribution trends were interpolated by triangulation using several locations within 30 to 50 miles (48.3 to 80.5 km) from the target site. Refer to **APPENDIX E** for the original data and the triangulation. The calculated free water surface evaporation for the month of August in Philadelphia, PA was 6.46 inches (164 mm), therefore, the annual evaporation was 35/6.46 = 542% that of the month of August.

Based on this data, the results from the experiment were extrapolated to assess the SCM's hydrologic performance. The SCM's evaporation behavior for one rain event in August was established experimentally; the number of rain events and the relationship between the month of August and the annual free water surface evaporation was assessed from historic records; therefore all data necessary for the projection was available. Each of the performed simulations was considered as a possible end-of-rain scenario with a different instantaneous water surface level. Total evaporation from the pervious concrete system was calculated for each of the six simulated scenarios using the following equation:

Equation 5.3 Annual evaporation of the SCM (no infiltration)

$$E_i = (\Sigma\ EVAP_i) * N * E_{FWS} / E_{FWS(AUG)}\ , \text{where}$$

E_i = annual evaporation from pervious concrete system with no infiltration, initial water level as in scenario *i*, in mm

$\Sigma\ EVAP_i$ = cumulative three-day evaporation from scenario *i*, in mm

N = average number of storms per month (assumed 5)

E_{FWS} = annual evaporation from free water surface, in mm

$E_{FWS(AUG)}$ = evaporation from free water surface in August, in mm

To put those estimates in perspective, the evaporation from a hypothetical SCM was presented as a percentage of the annual precipitation typical for the site. The average annual precipitation of 42.03 inches (1068 mm) reported for Philadelphia International Airport was used for this calculation (NOAA 1971-2000). The evaporation share was calculated by considering the loading ratio, i.e. the ratio of the total tributary drainage area to the pervious area. The Villanova pervious concrete system had a loading ratio of 3,920 ft^2 (364.4 m^2) to 1,500 ft^2 (139.4 m^2), or 2.61:1. The evaporation estimates for the hypothetical loading ratio of 1:1 was also provided. To compute the percentage of the evaporation share, the following equation was used:

Equation 5.4 Evaporation share (no infiltration)

(% of the annual SCM water budget) = E_i / [P * (A_T/A_P)] * 100, where

E_i = as previously defined

P = annual precipitation, in mm

A_T = total tributary drainage area, in m^2

A_P = pervious area, in m^2

A_T/A_P = loading ratio

Table 5.1 summarizes the annual evaporation estimates for six end-of-rain scenarios.

Table 5.1 Annual SCM evaporation estimates (no infiltration)

i, scenario ID	Initial depth to a water surface, inches (mm)	Σ EVAP$_i$, mm	N	E_{FWS}, mm	$E_{FWS(AUG)}$, mm	E_i, mm	P, mm	% of the annual SCM water budget	
								A_T/A_P = 1:1	A_T/A_P = 2.61:1
1	0 (0)	12.05	5	889	164	327	1068	30.6	11.7
2	1 (25)	10.00	5	889	164	271	1068	25.4	9.7
3*	3 (76)	5.85	5	889	164	159	1068	14.8	5.7
4	6 (152)	4.68	5	889	164	127	1068	11.9	4.6
5	10 (254)	3.66	5	889	164	99	1068	9.3	3.6
6	15 (381)	3.46	5	889	164	94	1068	8.8	3.4

NOTES:

* Session 3 had only two days worth of data due to equipment malfunction. Evaporation for the third day was calculated using Equation 5.2.

This analysis indicates that the evaporation share in the annual water budget from the Villanova pervious concrete SCM with no infiltration could range from 3.4 to 11.7 percent, depending on the initial depth to the ponded water surface. This share would be 8.8 to 30.6 percent if the drainage area was limited to the pervious pavement only (i.e. loading ratio of 1:1). Selecting a single value within this range that would be representative for the average annual evaporation share would depend on the distribution between the large storms, which produce saturated conditions, and the small storms, which result in the low water level conditions. To simplify the calculation it was assumed that 90% of the rainfall events have a total precipitation of less than one inch (25 mm) (typically assumed for the "green" SCM designs in the Philadelphia area) and the remaining 10% - greater or equal than one inch (25 mm), with the average value of 2 inches (51 mm). Since the storage capacity of the Villanova University SCM with an infiltration bed depth of 42 inches (1067 mm) was 2 inches (51 mm) of precipitation, 10% of the rain events would result in saturated conditions (Scenario 1) and the remaining 90% would result in water levels below influence zone (Scenario 6). Using a

weighted average calculation, the most representative value for the evaporation share in the Villanova SCM (no infiltration) annual water budget would be 11.7*0.1+3.4*0.9 = 4.2 percent. Using a similar analysis for the loading ratio of 1:1, the evaporation share would be 30.6*0.1+8.8*0.9 = 11.0 percent.

Revising these estimates to incorporate the infiltration rates typical for pervious pavement systems would reduce the evaporation share in a yearly water budget. If the infiltration rate is 0.5 inches/hour (13 mm/hour), which is the case for the Villanova pervious concrete system, the ponded water surface would recede from the saturated conditions to a level below the influence zone established at 10 inches (254mm) in just 20 hours. At the beginning of this process, evaporation rates are expected to match saturated conditions, while after 20 hours the rates are expected to match low water level conditions.

The calculations were performed to evaluate the evaporation behavior of the SCM with an infiltration rate of 0.5 inches per hour. Three-day evaporation rates were calculated. The base line for this estimate was evaporation from the simulation with water level below the influence zone, with adjustments for the variable water elevation within the influence zone. The calculation assumed variable daily evaporation rates during the first several hours it takes for the water to draw down from the initial conditions to the depth below the influence zone of 10 inches (254 mm). Evaporation for the remainder of the first day was prorated using the results for the simulation with the initial water level below the influence zone. The evaporation from day two and day three were assumed to be equal to the corresponding results from the simulation with the low water levels.

The data presented in **Figure 5.13** establishes the first day evaporation rates as a function of the initial depth to the ponded water surface. The abscissa had to be shifted one value to the left away from zero to enable power regression analysis.

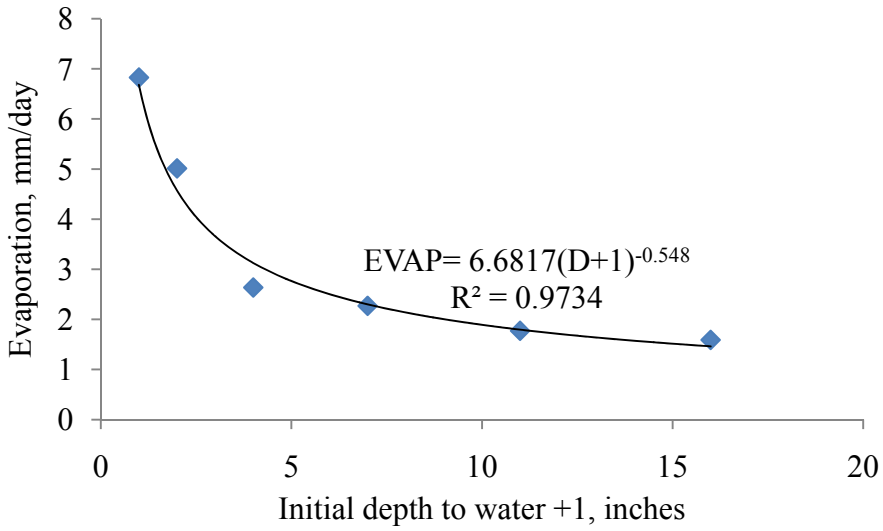

Figure 5.13 First day evaporation vs. initial depth

The relationship between the first day evaporation and the initial depth to water was established by the regression analysis and had the following form:

Equation 5.5 First day evaporation vs. depth

$$EVAP = 6.6817(D/25.4+1)^{-0.548}$$, where

EVAP = daily evaporation, in mm/day

D = initial depth to a ponded water surface, in mm

The equation was rearranged to incorporate receding water levels due to infiltration. Since the infiltration rates were constant at 0.5 inches/hour (12.7 mm/hour), a depth to the water surface was expressed using the time it took to reach this depth. The resulting equation is presented below.

Equation 5.6 First day evaporation vs. time

$$EVAP = 6.6817(t/2+1)^{-0.548}$$, where

EVAP = as previously defined

t = D (mm) / 12.7 (mm/hr) = time to reach the depth D, in hours

D = as previously defined

The cumulative evaporation from the initial depth to the water surface to a depth just below the influence zone was calculated by numerical integration using the following formula:

Equation 5.7 Cumulative evaporation within influence zone

$$\mathrm{E(a,b)} = 1/24 \int_{a}^{b} 6.6817 \left(\frac{t}{2}+1\right)^{-0.548} dt, \text{ where}$$

E(a,b) = cumulative evaporation from the hour a to the hour b, in mm

The cumulative three-day evaporation rate was calculated using the following equations.

Equation 5.8 Three-day evaporation, compensated for infiltration

$$\Sigma\ EVAP_i = E(a,b) + E'_1 + E_2 + E_3$$

$$E'_1 = E_1(24-(b-a))/24, \text{ where}$$

$\Sigma\ EVAP_i$ = three-day evaporation rates for initial water depth as in scenario *i*

E(a,b) = cumulative evaporation when the water levels within the influence zone, in mm

E'_1 = the remaining day 1 evaporation, in mm

E_2 = cumulative evaporation from day 2, in mm

E_3 = cumulative evaporation day 3, in mm

The results are summarized in **Table 5.2**.

Table 5.2 Three-day evaporation, compensated for infiltration

i, scenario ID	Initial depth to a water surface, inches (mm)	a-b, time to drain to 10" (254 mm), hrs	E(a,b), mm	Remaining hours for day 1	E_1, mm	E_2, mm	E_3, mm	E'_1, mm	$\Sigma EVAP_i$, mm
1	0 (0)	20	2.41	4	1.77	1.02	0.87	0.30	4.60
2	1 (25)	18	1.96	6	1.77	1.02	0.87	0.44	4.29
3	3 (76)	14	1.34	10	1.77	1.02	0.87	0.74	3.97
4	6 (152)	8	0.67	16	1.77	1.02	0.87	1.18	3.74
5	10 (254)	0	0	24	1.77	1.02	0.87	1.77	3.66
6	15 (381)	0	0	24	1.59	1.03	0.84	1.59	3.46

Using the three-day evaporation rates, the annual evaporation from the Villanova SCM was projected using **Equation 5.3**. Similar to the analysis performed for the hypothetical no-infiltration scenario, the results were evaluated as a percentage of the annual precipitation typical for the site using **Equation 5.4**. **Table 5.3** provides a summary of the results.

Table 5.3 Annual evaporation estimates (with infiltration)

i, scenario ID	Initial depth to a water surface, inches (mm)	$\Sigma EVAP_i$, mm	N	E_{FWS}, mm	$E_{FWS(AUG)}$, mm	E_i, mm	Annual precip, mm	% of the annual SCM water budget	
								A_T/A_P = 1:1	A_T/A_P = 2.61:1
1	0 (0)	4.60	5	889	164	125	1068	11.7	4.5
2	1 (25)	4.29	5	889	164	117	1068	10.9	4.2
3	3 (76)	3.97	5	889	164	108	1068	10.1	3.9
4	6 (152)	3.74	5	889	164	102	1068	9.5	3.6
5	10 (254)	3.66	5	889	164	99	1068	9.3	3.6
6	15 (381)	3.46	5	889	164	94	1068	8.8	3.4

Following the rain event distribution assumptions as described earlier in this section, the single most probable value representing the annual share of the evaporation in the SCM water budget was calculated. For the Villanova pervious concrete system with an infiltration rate of 0.5 inches/hour (13 mm/hour) the evaporation share was estimated as 3.7% of the annual water budget. This estimate would have been 9.1% percent if the loading ratio was 1:1.

Since the design of the Villanova SCM followed typical guidelines, it is reasonable to assume that other pervious concrete systems constructed per those design criteria would produce comparable evaporation rates in similar meteorological conditions. The actual evaporation share would vary greatly depending on the loading ratio at the particular site. The estimate provided for the loading ratio of 1:1 could be used as a starting point to predict the site-specific evaporation.

The hydrologic perspective analysis revealed that the role of evaporation in the annual water budget of the Villanova pervious concrete SCM is less than 4%, which is not very significant. However, it became evident that the design on the structure greatly affects evaporation behavior. The evaporation share is expected to be significant if the pervious concrete system is designed to promote water vapor transfer. Considerations for the design of pervious concrete systems that enhance the evaporation performance are presented in **Section 5.5.3** .

5.5.3 Considerations for the system design

It must be noted that design considerations and the recommendations provided herein were established by deduction from the experimental results and not substantiated by field evidence at this point.

As previously mentioned, the applicability of pervious concrete systems is currently limited to areas with underlying soils with relatively good infiltration capacity. These limitations are imposed by regulations developed with the premise that subsoil infiltration

is the only method for runoff release from the storage bed (not counting overflow from large storm events when the storage capacity is exceeded).

Site-specific constraints might be present in which infiltration is relatively poor due to low permeability of the subsoil. In some instances, rapid infiltration is undesirable, e.g. in areas with a high water table. In those instances, the use of pervious pavement systems as a means to reduce runoff volume would not be approved. It is believed that the applicability range of pervious pavement systems could be expanded by designing the structures to promote evaporation.

The experimental results from this work indicate that no pervious concrete system would be able release 100% of stored runoff exclusively by evaporation. While all the water from a shallow system would eventually evaporate, the rates might be too slow to prepare the system for the next rain event. Three days is a rule-of-thumb estimate for the dissipation of the stored runoff to recharge the bed for the next rain event (PADEP 2006). Three-day evaporation rates from the simulation with the initially saturated conditions were slightly over 12 mm (0.47 inches), expressed in the equivalent evaporation from a free water surface. This estimate, translated in terms of water surface drop in a pervious concrete with the porosity of 0.2, would amount to 60 mm (2.37 inches). Thus, a pervious concrete system with a depth of 60 mm (2.37 inches) would be able to empty in three days exclusively by evaporation. Since those estimates were performed for the month of August when the evaporation rates are higher than a yearly average, this depth is expected to be even shallower for the overall annual performance. Such a shallow system is unlikely to be feasible in current pervious pavement applications, mainly from a structural standpoint and freeze/thaw considerations.

Evaporation cannot single-handedly achieve the SCM hydrologic performance goals; however, it could play a substantial auxiliary role to supplement other runoff release mechanism(s) if a pervious pavement system is designed to promote evaporation. Several steps could be taken to enhance the evaporation performance.

- Building shallow structures with the total depth not exceeding the influence zone of 10 inches (254 mm) would greatly increase the evaporation rates.
- Limiting the tributary drainage area to the footprint of the structure itself would increase the effective evaporation area, and therefore, the share of the evaporation in the annual water budget.
- The storage beds should be sized to allow ponded water to be level or near-level with the pervious concrete surface for the design rainstorm event.
- If a pervious pavement surface is sloped, a benched design could be implemented below the concrete layer to maximize storage and evaporation by allowing the ponded water to be closer to the surface.
- The elevation of the overflow system weir should be as close to the pervious concrete surface as feasible to maintain a high water level, but prevent overflow through the pores in the concrete.
- It might be beneficial to control the overflow operation mode to accommodate the hydrologic performance goals of the SCM, which can vary seasonally. This could be achieved by regulating the weir elevation, which would allow for the control of the balance between evaporation and outflow. Also, an underdrain with a controllable shut-off valve could be utilized to allow for an additional outflow capacity as needed.

A design that maximizes the evaporation might have limitations in climates with sub-freezing winter temperatures due to the potential for freezing of the ponded water and subsequent frost heave and cracking of the concrete surface. In those instances, the overflow weir elevation might be lowered, which would result in increased overflow and lowering of the ponded water surface.

6. Conclusions

From a review of the current design practices, it was established that current pervious concrete SCM design guidelines do not account for evaporation. From a further literature review, no conclusive estimates on the evaporation from pervious concrete systems or

computational techniques that allow a designer to estimate the evaporation were found. It was concluded that the investigation of the evaporation behavior of the pervious concrete system at Villanova University could provide sufficient clues to estimate the evaporation share of an annual SCM water budget.

A bench-top experiment was designed and built to assess the evaporation performance using the Villanova pervious concrete SCM as a prototype. In contrast to the actual SCM, the apparatus did not feature an infiltration mechanism. A dynamic thermal response of the apparatus was calibrated to resemble that of a prototype on a typical clear-sky day in August. A solar simulator was designed and built for this purpose. Environmental parameters such as rainfall, wind, and relative humidity were simulated to match the field conditions. The apparatus was instrumented to monitor evaporation and the environmental parameters. The experimental program was designed to obtain a range of evaporation rates from a pervious pavement SCM with inhibited infiltration, which would result from different ponded water-level scenarios.

Qualitative parameterization was performed to identify the factors affecting evaporation rates from a pervious concrete system.

Six simulations with a variable initial depth to a ponded water surface were performed. The experimental data was processed and analyzed. The observed three-day evaporation rates varied from 3.5 mm to 12.1 mm (0.14 inches to 0.47 inches). The order of magnitude verification of the observed evaporation rates was performed with satisfactory results. A predictive empirical relationship between daily evaporation, initial depth to a water surface and the time elapsed since the last rain event was established. The scope of the predictions was limited to the first three days after the rain event occurring in August.

The observed evaporation behavior was discussed in detail and a qualitative sensitivity analysis was performed.

Year-round evaporation performance from a Villanova pervious concrete SCM was estimated using the experiment results using computational techniques to adjust for the infiltration, historical weather data, and published evaporation data from shallow open water bodies. The share of the evaporation from the SCM was found to depend on the initial depth to ponded water surface and a loading ratio. For the Villanova SCM with inhibited infiltration, the annual evaporation share was estimated as 4.2%. Adjusted for the infiltration rate, the evaporation share was estimated as 3.7%. If the Villanova SCM was designed with a loading ratio of 1:1, those estimates would be 11.0% (the infiltration inhibited) and 9.1% (adjusted for the infiltration).

It was theorized that other BMPs, similarly designed, would produce comparable evaporation rates when exposed to similar environmental conditions.

It was concluded that evaporation plays a measurable, but not a very significant role in pervious concrete systems designed for relatively rapid infiltration. However, this role could be significant if the systems were designed to promote the evaporation. It was concluded that designing for evaporation would expand the applicability range of pervious concrete systems. Several conceptual design considerations enhancing evaporation behavior were presented.

7. Future research

The experimental work and the conclusions presented here could be expanded both in breadth and in depth to deepen the understanding of the evaporation in pervious pavements and to confirm the hydrologic perspective analysis and design recommendations. Substantial work is required to complete the parameterization of the pervious pavement evaporation for all temperature regimes, meteorological conditions, media types and system configurations. Some of the proposed future work is outlined in this section.

Since the experimental setup was scaled in the horizontal direction, it is necessary to investigate scale-related effects, particularly, the near-wall affect on the evaporation

rates. This could be achieved by repeating the experiment with a variable diameter of the evaporative column and evaluating the resulting differences in the evaporation rates.

To gain more insight into the evaporation behavior, the experimental program might be extended to seven days per simulation to quantify the evaporation beyond the first three days.

Although the pervious concrete specifications call for a relatively narrow porosity range, it would be beneficial to establish a relationship between porosity and evaporation rates. Such a relationship could be established by running the simulations using the media with variable porosity in the applicable range.

It is important to evaluate the long-term evaporation performance of the pervious pavement systems. Since pervious surfaces might be susceptible to clogging, establishing the link between the degree of clogging and the resulting changes in the evaporation rates would allow one to assess the life-cycle evaporation performance more accurately.

Mineral deposition as a result of evaporation could contribute to clogging of the pervious surface, therefore effects of mineral deposition need to be investigated. Simulations with harvested rainwater performed in a cyclic manner with enough repetitions might help to evaluate the significance of this phenomenon.

An experimental program, similar to the one described here, is being planned to assess the evaporation performance of porous asphalt systems. The top layer of the experimental apparatus will be replaced with a pre-cast porous asphalt specimen and the experimental program repeated.

A full-scale field study of a pervious pavement SCM built to promote evaporation might be the best way to evaluate year-round evaporation performance. However, measuring in-situ evaporation is likely to be the most challenging aspect of such an undertaking.

8. Bibliography

ASTM. *Standard Practice for Sampling Freshly Mixed Concrete.* West Conshohocken, PA: DOI: 10.1520/C0172-10, 2010.

Barbis, J., and A.L. Welker. "Stormwater temperature mitigation beneath porous pavements." *Proceedings of the World Environmental and Water Resources Congress 2010, May 20-24.* Providence, RI, 2010.

Ferguson, B. K. *Porous Pavements.* Boca Raton, FL: CRC Press, 2005.

Jeffers, P.A. *Water Quantity Comparison of Pervious Concrete and Porous Asphalt Products for Infiltration Best Management Practices, master degree thesis, Villanova University.* Villanova, PA, 2009.

Kevern, J. T., V.R. Schaefer, and K. Wang. "Temperature Behavior of a Pervious Concrete System." *Transportation Research Record: Journal of the Transportation Research Board, No. 2098*, 2009: 94-101.

MathWorks. *MATLAB R2010a.* 2010.

Mendel Weather Station. 2010. www.wunderground.com/weatherstation/WXDailyHistory.asp?ID=KPAVILLA1 (accessed January 12, 2011).

Microsoft. *MS Office Excel.* 2007.

NOAA. *Online Weather Data for Philadelphia International Airport.* 1971-2000. www.weather.gov/climate/xmacis.php?wfo=phi (accessed January 21, 2011).

NOAA. "Technical Report NWS 33, Evaporation Atlas for the Continuous 48 United States." Washington DC, 1982.

NOAA. "Technical Report NWS 34, Mean Monthly, Seasonal, and Annual Pan Evaporation for the United States." Washington DC, 1982.

Nofziger, D. L., and J. Wu. "SoilTemperature V2005.05.04." Stillwater, Oklahoma: Oklahoma State University, 2005.

PADEP. *Pennsylvania Stormwater BMP Manual.* PA Department of Environmental Protection, Bureau of Watershed Management, 2006.

SPSS. *SPSS 16.0.* 2010.

Starke, P., P. Göbel, and W.G. Coldewey. "Urban Evaporation Rates For Water-Permeable Pavements." *Water Science & Technology*, 2010: 1161-1169.

Tennis, P. D., M. L. Leming, and D. J. Akers. *Pervious Concrete Pavements.* Skokie, IL: Portland Cement Association, 2004.

Viessman, W., and G. L. Lewis. *Introduction to Hydrology, 5th edition.* Upper Saddle River, NJ: Prentice Hall, 2003.

9. Appendices

APPENDIX A

Pervious concrete mix design, performed by Dr. F. Hampton of Villanova University

Mix design for the pervious concrete batch was as follows (proportions by weight):

Coarse aggregate	Portland Cement	Water
4.67	1	0.4

APPENDIX B

Aggregate gradation analysis; used to build the stone bed for the experiment

12/10/2010 13:58 6102510184 CATANACH LAB PAGE 02

Glasgow, Inc.
Catanach Lab

Contractor	
Project	
Date	Typical

Supplier	GLA15A14: Catanach
Tech.	Bostelle

57 Gradation

Sieve	% Pass *Typical*	Spec
1 1/2"	*100*	100
1 "	*98.0*	95-100
3/4"	*79.3*	
1/2 "	*38.0*	25-60
3/8"	*17.9*	
# 4	*4.0*	0 - 10
# 8	*2.0*	0 - 5
Wash	*0.65*	0 - 2

Vincent J. Galletti
Quality Control
Glasgow Inc.

APPENDIX C

Algorithm of the solar simulator operation

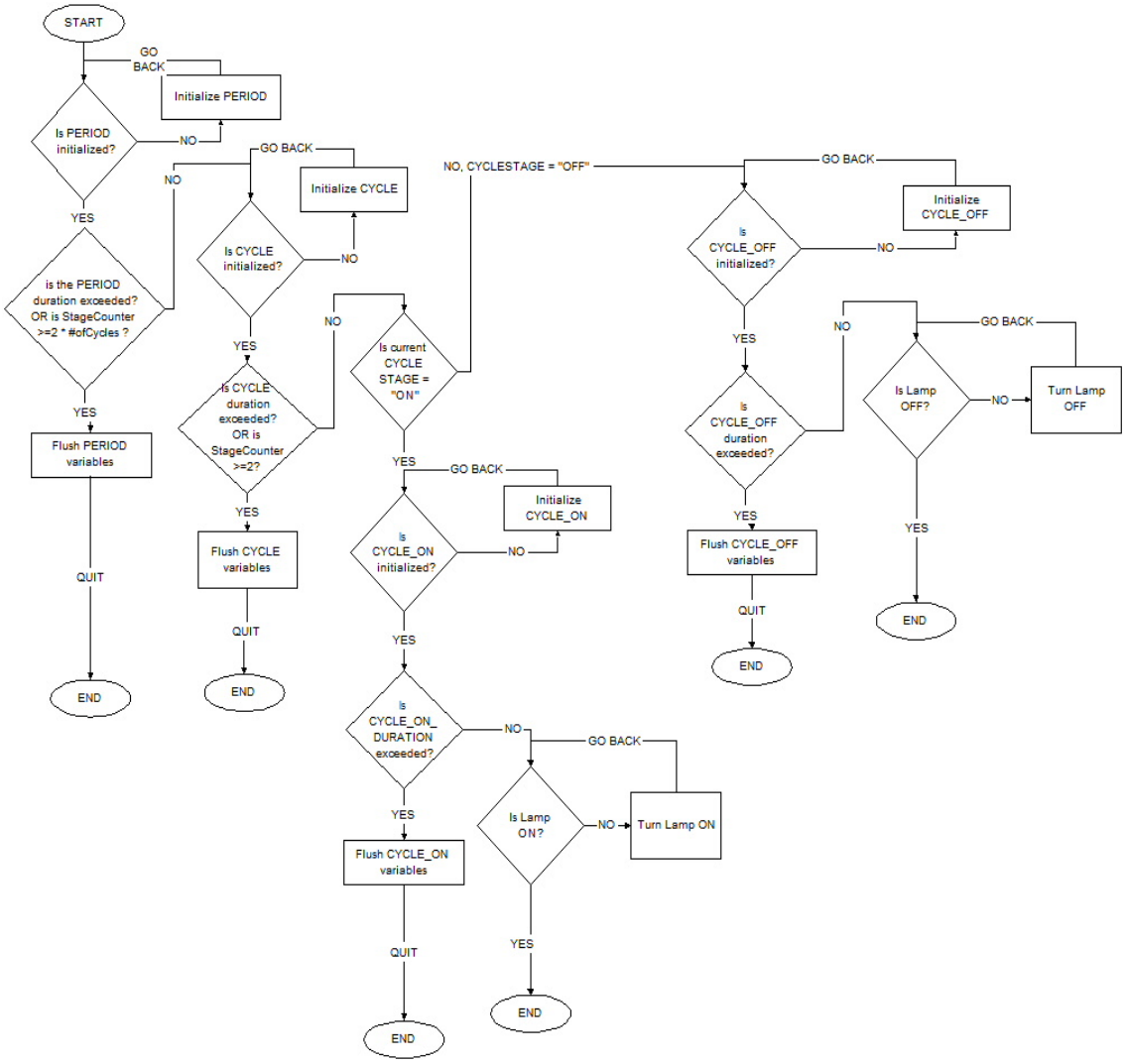

APPENDIX D

The complete datasets integrated over 2-hour period

Initial depth to the water surface: 0 inches (0 mm) (i.e. saturated conditions)

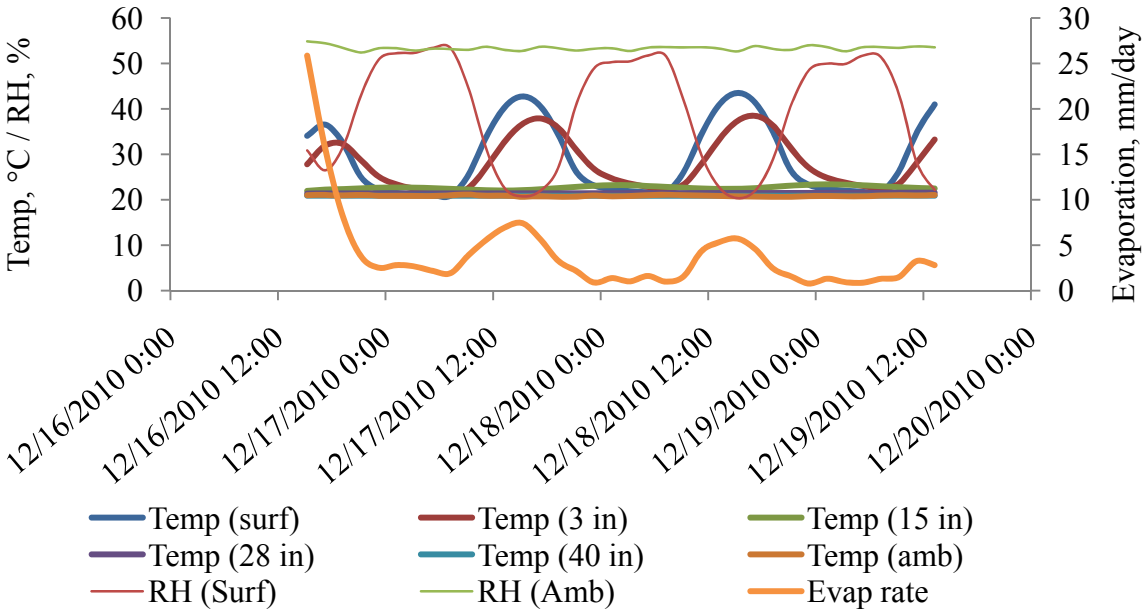

Initial depth to the water surface: 1 inch (25 mm)

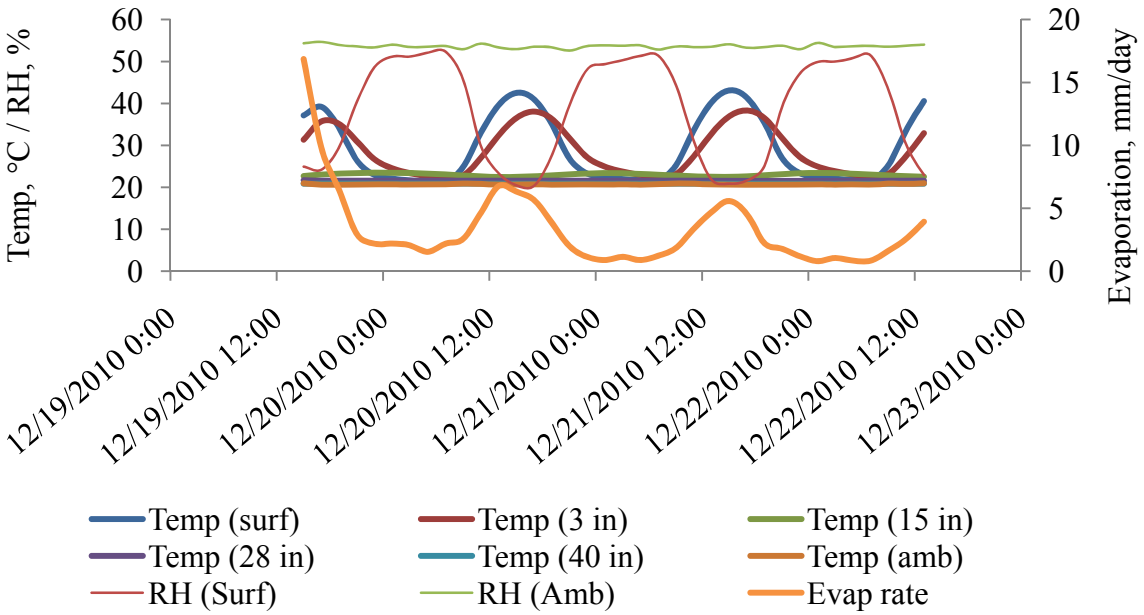

Initial depth to the water surface: 3 inches (76 mm)

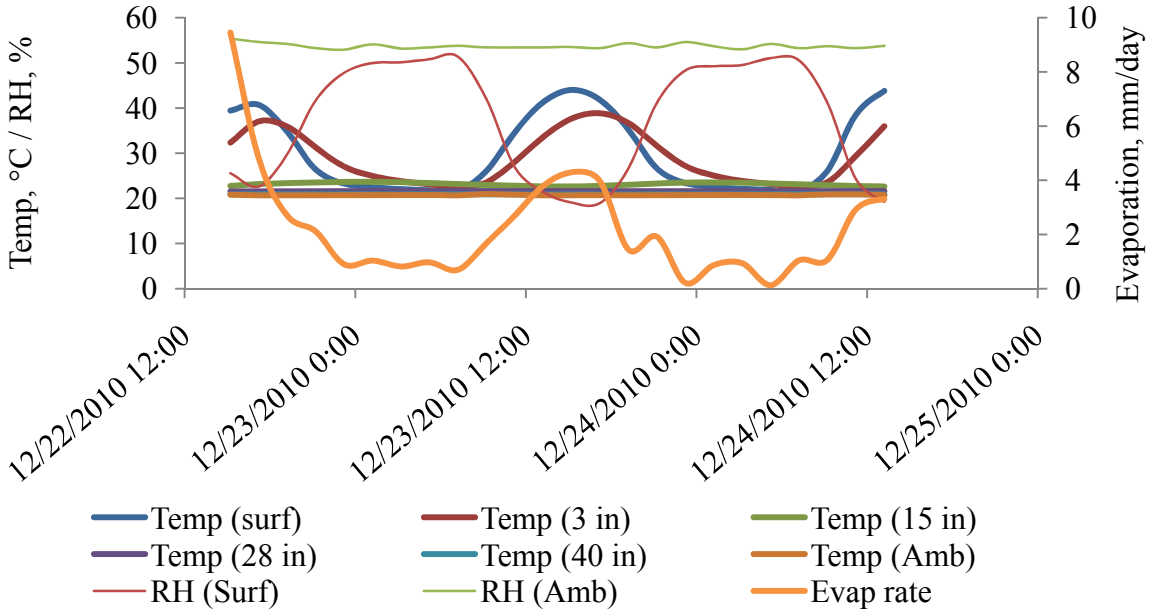

Initial depth to the water surface: 6 inches (152 mm)

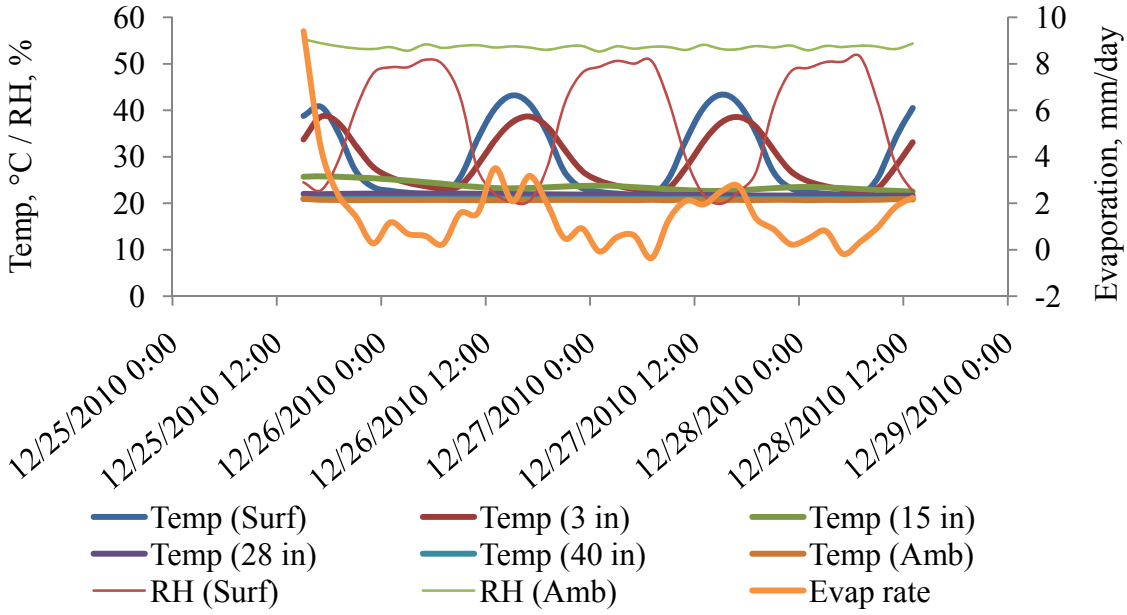

Initial depth to the water surface: 10 inches (254 mm)

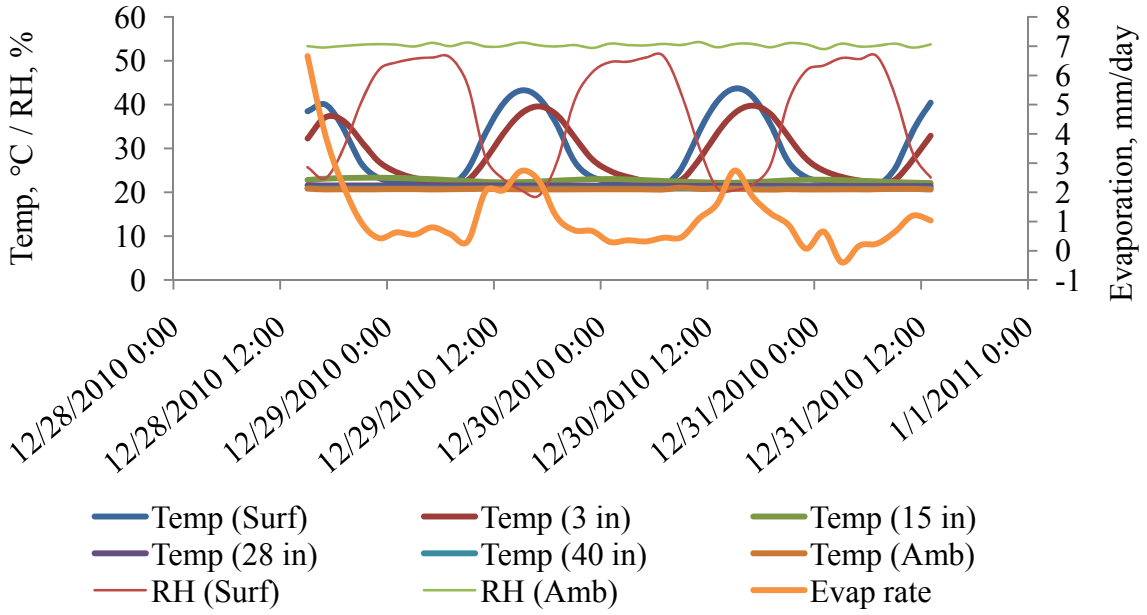

Initial depth to the water surface: 15 inches (381 mm)

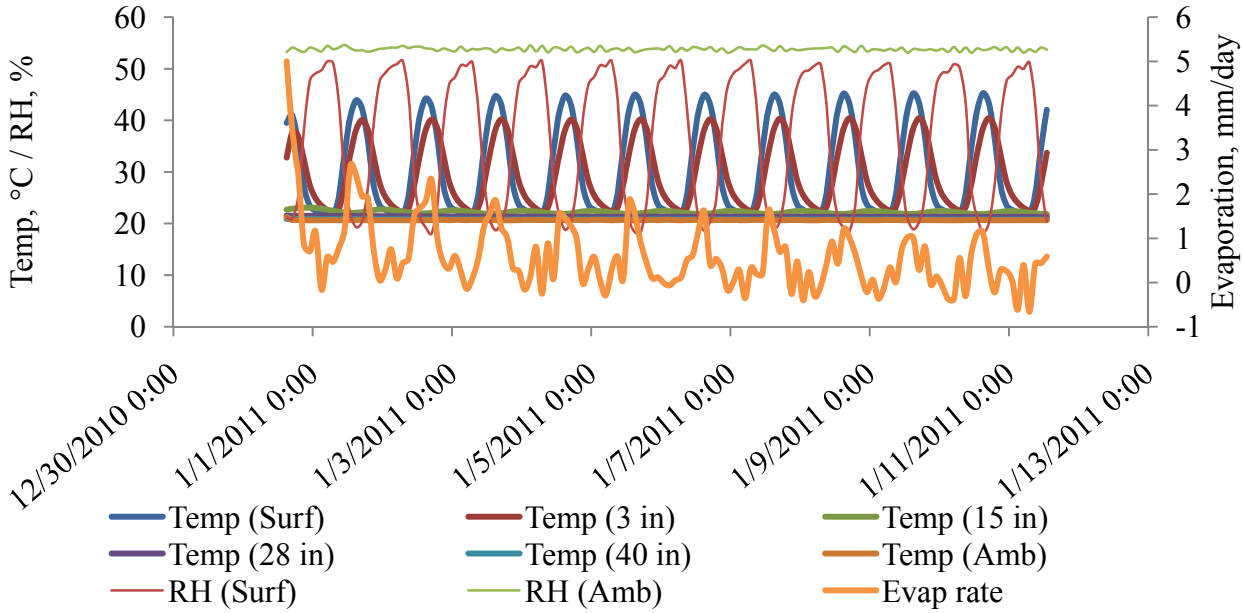

APPENDIX E

Free water surface evaporation: data and triangulation

NOAA TR-34: CLASS A PAN EVAPORATION, Monthly distribution, in inches/month													
Location / Distance from the target site	**Jan**	**Feb**	**Mar**	**Apr**	**May**	**Jun**	**Jul**	**Aug**	**Sep**	**Oct**	**Nov**	**Dec**	**Year**
NewArk, DE / 34 mi SW	0	0	0	0	5.17	6	6.39	5.59	4	0	0	0	27.15
Plesantville, NJ / 58 mi SE	0	0	0	4.15	5.63	5.85	6.58	5.67	4.01	2.68	1.95	0	36.52
New Brunswick, NJ / 54 mi NE	0	0	0	0	5.81	6.51	8.33	7.14	4.54	3.04	0	0	35.37
Landsville, PA / 55 mi W	0	0	0	0	5.74	6.61	7.17	5.91	4.31	2.89	0	0	32.63
Triangulated average / 0 mi	**0**	**0**	**0**	**1.0**	**5.6**	**6.2**	**7.1**	**6.1**	**4.2**	**2.2**	**0.5**	**0**	**32.9**
Triangulated distribution, % of annual / 0 mi	**0**	**0**	**0**	**3.2**	**17.0**	**19.0**	**21.6**	**18.5**	**12.8**	**6.5**	**1.5**	**0**	**100**

NOAA TR-33: FWS EVAPORATION for Philadelphia													
Parameter / Data source	**Jan**	**Feb**	**Mar**	**Apr**	**May**	**Jun**	**Jul**	**Aug**	**Sep**	**Oct**	**Nov**	**Dec**	**Year**
Annual FWS evap / Evaporation map													35
FWS evap, inches per month / Triangulation	0	0	0	1.10	5.94	6.64	7.57	6.46	4.48	2.29	0.52	0	35
FWS evap, mm perday / Triangulation	0	0	0	0.9	4.9	5.5	6.3	5.4	3.7	1.9	0.4	0	889
Distribution, % of August / Triangulation	**0**	**0**	**0**	**17.1**	**91.9**	**102.7**	**117.1**	**100.0**	**69.4**	**35.4**	**8.0**	**0**	**541.6**